

คุณลักษณะของหัววัดรังสีชนิดเพอร์และประสิทธิภาพของหัววัดนี้ในลำรังสีโฟตอนขนาดเล็ก



นายปญา ทรรธานนท์

## สถาบันวิทยบริการ จุฬาลงกรณ์มหาวิทยาลัย

วิทยานิพนธ์นี้เป็นส่วนหนึ่งของการศึกษาตามหลักสูตรปริญญาวิทยาศาสตรมหาบัณฑิต

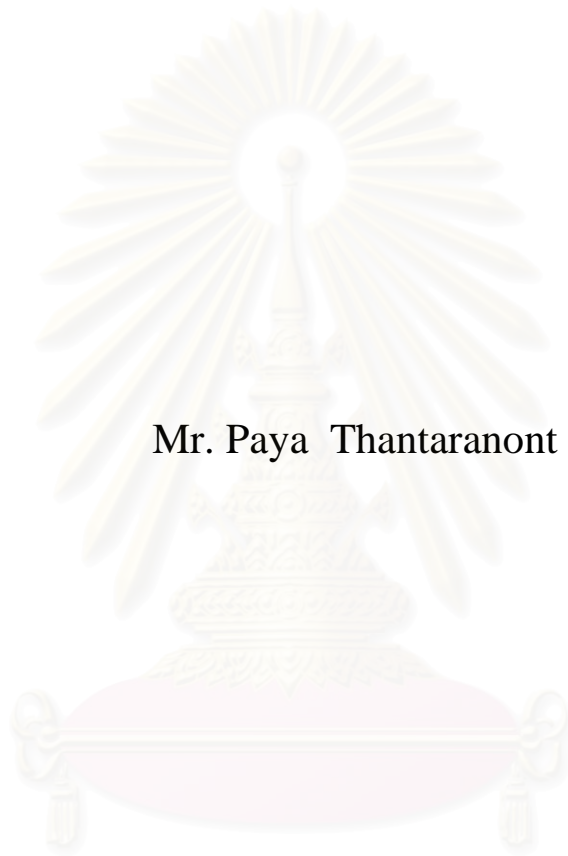
สาขาวิชาद्याเวทศาสตร์ ภาควิชารังสีวิทยา

คณะแพทยศาสตร์ จุฬาลงกรณ์มหาวิทยาลัย

ปีการศึกษา 2551

ลิขสิทธิ์ของจุฬาลงกรณ์มหาวิทยาลัย

THE CHARACTERISTICS OF DIAMOND DETECTOR AND  
ITS PERFORMANCE IN SMALL PHOTON BEAMS



Mr. Paya Thantaranont

สถาบันวิทยบริการ

A Thesis Submitted in Partial Fulfillment of the Requirements  
for the Degree of Master of Science Program in Medical Imaging

Department of Radiology

Faculty of Medicine

Chulalongkorn University

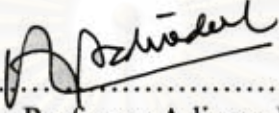
Academic Year 2008

Copyright of Chulalongkorn University

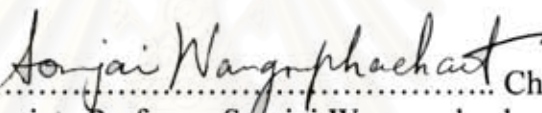
Thesis Title THE CHARACTERISTICS OF DIAMOND  
DETECTOR AND ITS PERFORMANCE IN SMALL  
PHOTON BEAMS  
By Mr.Paya Thantaranont  
Field of Study Medical Imaging  
Advisor Associate Professor Sivalee Suriyapee

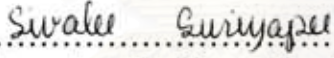
---

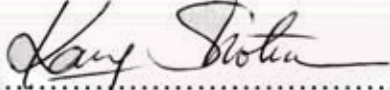
Accepted by the Faculty of Medicine, Chulalongkorn University in  
Partial Fulfillment of the Requirements for the Master's Degree

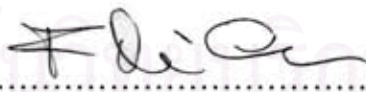
  
..... Dean of the Faculty of Medicine  
(Associate Professor Adisorn Patradul, M.D.)

THESIS COMMITTEE

  
..... Chairman  
(Associate Professor Somjai Wangsuphachart, M.D.)

  
..... Advisor  
(Associate Professor Sivalee Suriyapee)

  
..... Examiner  
(Associate Professor Kanjana Shotelersuk, M.D.)

  
..... External Examiner  
(Professor Franco Milano, Ph.D.)

สอว.ม.ค.ร.  
จุฬาลงกรณ์มหาวิทยาลัย

ปญญา ทรรทรานนท์ :คุณลักษณะของหัววัดรังสีชนิดเพชรและประสิทธิภาพของ  
หัววัดนี้ในลำรังสีโฟตอนขนาดเล็ก. (THE CHARACTERISTICS OF DIAMOND  
DETECTOR AND ITS PERFORMANCE IN SMALL PHOTON BEAMS) อ.ที่ปรึกษา  
วิทยานิพนธ์หลัก :รศ.ศิวลี สุริยาปี, 65 หน้า.

หัววัดรังสีในอุดมคติสำหรับวัดลำรังสีโฟตอนขนาดเล็กควรมีคุณสมบัติที่มีความไวต่อการวัดรังสีสูง มีความละเอียดเชิงระยะสูง มีการตอบสนองที่เสถียร และสมมูลกับเนื้อเยื่อ การศึกษานี้มีวัตถุประสงค์เพื่อหาคุณลักษณะทางการวัดรังสีของหัววัดชนิดเพชรของพีทีดับเบิลยู รุ่น 60003 และแสดงประสิทธิภาพในการวัดลำรังสีโฟตอนขนาดเล็ก 6 เมกะอิเล็กตรอนโวลต์ โดยในการศึกษาหาคุณลักษณะประกอบด้วย ผลของโพลาไรเซชัน, ความสามารถในการวัดซ้ำและความสม่ำเสมอของสัญญาณ, การตอบสนองของหัววัดต่อปริมาณรังสีที่ได้รับ, ผลของอัตราปริมาณรังสี, พลังงาน, และทิศทางของลำรังสีโฟตอนต่อการตอบสนองของหัววัด ประสิทธิภาพของหัววัดประเมินโดย การวัดเอาท์พุทแพคเตอร์, เดปท์โดสเคิร์ฟ และ บีมโปรไฟล์ ในลำรังสีขนาด  $1.5 \times 1.5 \times 10^{-10}$  ตร.ซม. โดยนำผลที่ได้เปรียบเทียบกับผลที่ได้จากการวัดโดย ซิลิคอน ไดโอด ชนิดพีไอพี และ ไอออนในเรซินแรมเบอร์ ขนาด 0.13 ลบ.ซม. หรือ ซีซี13 ของบริษัทแกนดิทรอนนิคเวลฮอเฟอร์

ผลที่ได้จากการศึกษา พบว่าปริมาณรังสีก่อนการฉาย ที่แก้ผลของโพลาไรเซชันและทำให้การตอบสนองของหัววัดเสถียร เท่ากับ 5 เกรย์ และ หลังจากเสถียรแล้วความคลาดเคลื่อนของการตอบสนองในการวัดซ้ำ อยู่ภายใน 0.16% และความสม่ำเสมอของการตอบสนองจากการวัดสัปดาห์ละ 1 ครั้ง ตลอดเวลา 1 เดือน เท่ากับ 0.4%, การตอบสนองของหัววัดเป็นเส้นตรงต่อปริมาณรังสีที่ได้รับในช่วง 1-400 เซนติเกรย์, อัตราส่วนของการตอบสนองของหัววัดชนิดเพชรต่อไอออนในเรซินแรมเบอร์ เท่ากับ 1.008 ถึง 0.995 ในช่วงของอัตราปริมาณรังสี 1.58 ถึง 4.96 เกรย์ต่ออนาที่ นอกจากนี้พบว่าการตอบสนองของหัววัดชนิดเพชรไม่ขึ้นกับพลังงานของรังสี แต่ขึ้นกับทิศทางของลำรังสีเล็กน้อย ด้านประสิทธิภาพพบว่าเอาท์พุทแพคเตอร์ที่ได้จากการวัดโดยหัววัดชนิดเพชร ใกล้เคียงกับที่วัดจากซีซี13และซิลิคอนไดโอดเมื่อลำรังสีใหญ่กว่า  $2 \times 2$  ตร.ซม. โดยปริมาณที่ได้จากหัววัดชนิดเพชรจะสูงกว่าและแตกต่างจากของ ซีซี13 มากขึ้นถึง 2.3% ที่ขนาด  $1.5 \times 1.5$  ตร.ซม. สำหรับการวัดเดปท์โดสเคิร์ฟ ความแตกต่างระหว่างหัววัดชนิดเพชรและชนิดอื่นมากกว่า 2% ที่ความลึกมากกว่า 15 ซม. สำหรับการวัดบีมโปรไฟล์ พบว่า ความกว้างของลำรังสีขนาด  $10 \times 10$  ลบ.ซม. ที่ได้จากหัววัดชนิดเพชรใกล้เคียงกับความกว้างของลำรังสีจากหัววัดอื่น แต่จะมีขนาดใหญ่ว่างกว่าความกว้างของลำรังสีจากหัววัดอื่น เมื่อลำรังสีมีขนาดเล็ก สำหรับขนาดของเงามัวที่ได้จากหัววัดชนิดเพชรจะกว้างกว่าของที่ได้จากซิลิคอนไดโอด แต่แคบกว่าที่ได้จากซีซี13 ในทุกขนาดลำรังสีที่ทำการศึกษา

จากการศึกษาครั้งนี้พบว่า หัววัดรังสีชนิดเพชรมีคุณลักษณะและประสิทธิภาพที่เหมาะสมในการวัดปริมาณทางรังสีขนาดเล็ก และด้วยคุณสมบัติของเพชรที่ใกล้เคียงสมมูลกับเนื้อเยื่อ ทำให้หัววัดรังสีชนิดเพชรเหนือกว่าซิลิคอนไดโอดอย่างไรก็ตาม ผู้ใช้ควรใส่ใจต่อปริมาณรังสีก่อนการฉาย เนื่องจากเกี่ยวข้องกับความเสี่ยงของการตอบสนองของหัววัด

ภาควิชา.....รังสีวิทยา..... ลายมือชื่อนิสิต..... ปุณฯ ทรรทรานนท์  
สาขาวิชา.....ฉายาเวชศาสตร์..... ลายมือชื่ออ.ที่ปรึกษาวิทยานิพนธ์หลัก.....ศิวลี สุริยาปี  
ปีการศึกษา.....2551.....



# #5074794230 : MAJOR MEDICAL IMAGING  
 KEYWORDS : DIAMOND DETECTOR / SMALL PHOTON BEAM /  
 DOSIMETRY / SMALL FIELD MEASUREMENT.

PAYA THANTARANONT : THE CHARACTERISTICS OF DIAMOND  
 DETECTOR AND ITS PERFORMANCE IN SMALL PHOTON BEAMS.  
 ADVISOR : ASSOC.PROF. SIVALEE SURIYAPEE, 65 pp.

An ideal radiation detector for small photon beam should have the properties of high radiation sensitivity, high spatial resolution, constant response and soft tissue equivalent. The objectives of this study were to investigate the characteristics of PTW Riga diamond detector type 60003 and evaluate its performance in small fields of 6 MV photon beams. The characteristics of diamond detector were studied for polarization effect, repeatability, reproducibility and linearity of response, dependence on; dose-rate, beam energy, and direction. Performance of diamond detector was compared with those of Scanditronix Wellhofer p-type silicon diode and 0.13 cc ionization chamber (CC13) by measurements for field sizes of  $1.5 \times 1.5$ - $10 \times 10$  cm<sup>2</sup> which included output factors (OF), percentage depth doses (PDD), and beam profiles.

Pre-irradiation dose of 5 Gy was required to solve the polarization effect and stabilize detector response. After pre-irradiation, the standard deviation was 0.16% in 10 repeated measurements and 0.4% for reproducibility in 1 month, 1 week apart. Diamond detector showed good linearity of response with the dose range studied of 1-400 cGy. The diamond to ion chamber response ratio were 1.008 to 0.995 for dose-rate varied from 1.58 to 4.69 Gy/min. Diamond detector showed no dependence on beam energy, slightly dependence on beam direction. Output factors measured by diamond detector were comparable with that measured by diode and CC13 for the field size greater than  $2 \times 2$  cm<sup>2</sup> and increasing to 2.3% for  $1.5 \times 1.5$  cm<sup>2</sup> with higher dose by diamond detector. For PDD measurements, the deviations between diamond-diode and diamond-CC13 were higher than 2% at the depth deeper than 15 cm. For beam profile measurement, radiological width (RW50) measured by diamond detector were comparable with those by diode and CC13 for  $10 \times 10$  cm<sup>2</sup> field size and larger than the others for small field size. Penumbra width (80-20%) measured by diamond detector was also larger than diode but smaller than CC13 for all field sizes study.

For small field of photon beam, the diamond detector has suitable characteristics and performance for dosimetric applications. Due to its tissue equivalent property, the diamond detector is superior to the diode. However, the user should be attending to pre-irradiation process which relates to the stability of detector response.

Department : .....Radiology.....

Student's Signature

*Paya Thantaranont*

Field of Study : ....Medical Imaging.....

Advisor's Signature

*Sivalee Suriyapee*

Academic Year : ...2008.....

## ACKNOWLEDGEMENTS

I would like express gratitude to my advisor Assoc.Prof.Sivalee Suriyapee for her guidance, invaluable advice, supervision, and constructive comments. She was always there to listen and to give advice. She also taught me how to think and work as a good physicist.

A special thanks goes to my co-advisor, Mr.Isra Israngkul-Na-Ayuthaya, who is most responsible for helping me complete this thesis. He also gave me a good advice in photographic issue.

I would like to thank Mr.Taweap Sanghangthum, Mr.Sornjarod Oonsiri, Ms.Pantiwa Insang, Ms.Chotika Jampangern, and all of the staff at Division of Radiation Oncology, Chulalongkorn University and KCMH for helpful assistance and advice.

I would like to deeply thank Assoc.Prof.Anchali Krisanachinda, Director of M.Sc. in Medical Imaging Program, Chulalongkorn University for her kindness, invaluable suggestion and constructive comments.

Besides my advisors, I would like to thank the rest of my thesis committee: Assoc.Prof. Somjai Wangsuphachart, Assoc.Prof. Kanjana Shotelersuk, and Prof.Franco Milano for their kindness and valuable suggestion.

I would like to thank Dr.Kitisak Thepsuwan, Director of Chonburi Cancer Center and Ms.Pattama Na-Nakorn, physicist for education opportunity and financial support.

Last, I thank my family, Sumon and Saitong Thantaranont for giving me life, for educating me with aspects from both sciences and arts, for unconditional support. The usefulness of this thesis, I dedicate to them and all the teachers.

สถาบันวิทยบริการ  
จุฬาลงกรณ์มหาวิทยาลัย

# CONTENTS

	Page
ABSTRACT (THAI).....	iv
ABSTRACT (ENGLISH).....	v
ACKNOWLEDGEMENTS.....	vi
CONTENTS.....	vii
LIST OF TABLES.....	ix
LIST OF FIGURES.....	xi
LIST OF ABBREVIATIONS.....	xiv
<b>CHAPTER I INTRODUCTION.....</b>	<b>1</b>
1.1 Background and rationale.....	1
1.2 Research objectives.....	2
<b>CHAPTER 2 LITERATURE REVIEWS.....</b>	
2.1 Theories.....	3
2.1.1 Radiation detection.....	3
2.1.2 Ionization chamber.....	3
2.1.3 Semiconductor detector.....	5
2.1.4 Diamond detector.....	9
2.1.5 Dose Distribution, Beam output and Beam profile.....	12
2.2 Related literature review.....	20
<b>CHAPTER 3 RESEARCH METHODOLOGY.....</b>	<b>22</b>
3.1 Research design.....	22
3.2 Research design model.....	22
3.3 Conceptual framework.....	22
3.4 Keywords.....	23
3.5 Materials.....	23
3.5.1 Diamond detector.....	23
3.5.2 Linear accelerator.....	24
3.5.3 Phantom.....	25
3.5.4 Electrometer.....	26
3.5.5 Adaptor cable.....	26
3.5.6 Ionization chamber.....	27
3.5.7 Silicon diode detector.....	27

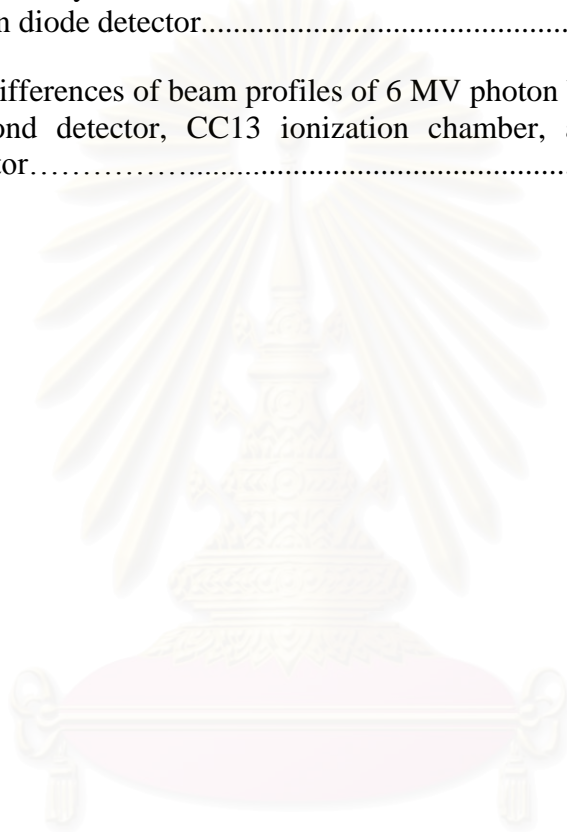
3.5.8 Build up cap.....	27
3.6 Methods.....	28
3.6.1 Characteristics of diamond detector.....	28
3.6.2 Performance of diamond detector.....	33
3.7 Data collection.....	36
3.8 Data analysis.....	36
3.8.1 Characteristics of diamond detector.....	36
3.8.2 Performance of diamond detector.....	36
3.8.3 Uncertainty evaluation.....	38
3.9 Expected benefit and application.....	39
3.10 Ethic consideration.....	39
<b>CHAPTER 4 RESULTS.....</b>	<b>40</b>
4.1 Characteristics of diamond detector.....	40
4.1.1 Polarization effect.....	40
4.1.2 Repeatability and reproducibility.....	43
4.1.3 Linearity of response.....	44
4.1.4 Dose rate dependence.....	46
4.1.5 Beam energy dependence.....	47
4.1.6 Directional dependence.....	48
4.2 Performance of diamond detector.....	50
4.2.1 Output measurement.....	50
4.2.2 Depth dose curves measurement.....	51
4.2.3 Beam profile measurement.....	56
<b>CHAPTER 5 DISCUSSION AND CONCLUSION.....</b>	<b>60</b>
5.1 Discussion.....	60
5.1.1 Characteristics of diamond detector.....	60
5.1.2 Performance of diamond detector.....	61
5.2 Conclusion.....	62
5.2 Recommendation.....	62
<b>REFERENCES.....</b>	<b>63</b>
<b>VITAE.....</b>	<b>65</b>



## LIST OF TABLES

<b>Table</b>		<b>Page</b>
2.1	Radiation effects used in the detection and measurement of radiation	3
2.2	Comparison of properties of natural diamond, CVD diamond, silicon diode, and MOSFET.....	11
3.1	Physical and operating parameters of the PTW diamond detector.....	23
3.2	Criteria in characteristics study.....	36
3.3	Summary of regions of validity of the $\delta_1$ - $\delta_4$ , radiological width RW50, and beam fringe $\delta_{50-90}$ criteria.....	38
4.1	Variations of diamond detector sensitivity with the accumulated dose at depth of 1.5 cm for 6 MV photon beams, given in 0.5 Gy steps, SSD = 100 cm.....	41
4.2	Variations of diamond detector sensitivity of 10 repeated measurements after pre-irradiation. Performed once a week for 6 MV photon beams, 10×10 cm <sup>2</sup> field size at depth of 1.5 cm, SSD = 100 cm.....	43
4.3	Variations of diamond detector response to given dose of 1-400 cGy for 6 MV photon beams, 10×10 cm <sup>2</sup> field size, 1.5 cm depth, SSD = 100 cm.....	45
4.4	Variations of diamond detector sensitivity versus dose rate, for 6 MV photon beams, 10×10 cm <sup>2</sup> field size at depth of 1.5 cm.....	47
4.5	Response of diamond detector and reference chamber for 6 and 10 MV photon beam, field size of 10×10 cm <sup>2</sup> at depth of 10 cm, SSD = 100 cm, and given dose of 100 MU.....	47
4.6	Variations of diamond detector response to the beam directions, in 6 MV photon beams, 10×10 cm <sup>2</sup> field size, source to the center of detector = 100 cm. (N/P = Not Perform).....	49
4.7	Output factors of 6 MV photon beam obtained by diamond detector, CC13 ionization chamber, and silicon diode detector, in field size of 10×10 cm <sup>2</sup> at depth of 1.5 cm, SSD = 100 cm.....	51
4.8	The differences of build up region of depth dose curves of 6 MV photon beams obtained by diamond detector compared with those obtained by CC13 and silicon diode detector. The sign (+) indicates to deeper and the sign (-) indicates to more surface than data of diamond detector.....	54

Table	Page	
4.9	The differences of descending region of depth dose curves of 6 MV photon beams obtained by diamond detector compared with those obtained by CC13 and silicon diode detector. The sign (+) indicates to higher and the sign (-) indicates to lower than data of diamond detector.....	55
4.10	Comparison of components of beam profiles of 6 MV photon beams obtained by diamond detector, CC13 ionization chamber, and silicon diode detector.....	56
4.11	The differences of beam profiles of 6 MV photon beams obtained by diamond detector, CC13 ionization chamber, and silicon diode detector.....	57



สถาบันวิทยบริการ  
จุฬาลงกรณ์มหาวิทยาลัย

## LIST OF FIGURES

Figure		Page
1.1	PTW Riga natural diamond detector type 60003.....	1
2.1	Schematic diagrams illustrating the nature of the thimble ionization chamber. (A) Air shell with air cavity. (B) Solid air shell with air cavity. (C) The thimble chamber.....	4
2.2	Basic circuits for an ionization chamber.....	5
2.3	Difference type of band structure.....	6
2.4	The radiation detection principle of silicon diode.....	7
2.5	Diagram of the <i>n</i> -type MOSFET principle .....	8
2.6	Structure of diamond crystal .....	9
2.7	Diagram of the PTW diamond detector structure and its x-ray image..	10
2.8	Illustration of polarization effect.....	12
2.9	Percentage depth dose is $(Dd/Dd_0) \times 100$ , where <i>d</i> is any depth and <i>d</i> <sub>0</sub> is reference depth of maximum dose .....	13
2.10	Central axis depth dose distribution for difference quality photon beams. Field size 10×10 cm <sup>2</sup> ; SSD = 100 cm for all beam except for 3.0 mm Cu HVL, SSD = 50 cm.....	14
2.11	Schematic plot of absorbed dose and kerma as functions of depth.....	15
2.12	Plot of relative dose rate as inverse square law function of distance from a point source. Reference distance = 80 cm.....	17
2.13	Arrangement for measuring (A) <i>S<sub>c</sub></i> and (B) <i>S<sub>c,p</sub></i> .....	18
3.1	Research design model.....	22
3.2	Conceptual frameworks.....	22
3.3	Diagram of the diamond detector.....	23
3.4	Linear accelerator (Varian Clinac 21 EX).....	24
3.5	Solid water phantoms.....	25
3.6	Blue phantom.....	25

<b>Figure</b>	<b>Page</b>
3.7 Dose1 electrometer.....	26
3.8 PTW adapter cable.....	26
3.9 The detectors used in this study; (Left: Silicon diode, Middle: Diamond detector, Right: CC13).....	27
3.10 Build up cap.....	27
3.11 Diagram of typical set-up in characteristics studies.....	28
3.12 Variations of dose rate as inverse square law function to SSD.....	30
3.13 Set-up of the dose rate dependence study.....	31
3.14 Diamond detector configurations in directional dependence study; (A) Perpendicular to central beam axis, (B) Parallel to central beam axis.....	32
3.15 Regions of validity of the criteria $\delta_1$ - $\delta_4$ , radiological width $RW_{50}$ , and beam fringe $\delta_{50-90}$ in (A) depth dose curve and (B) beam profile.....	37
4.1 Variations of diamond detector sensitivity with the accumulated dose at depth of 1.5 cm for 6 MV photon beams, given in 0.5 Gy steps, SSD = 100 cm.....	40
4.2 Variations of diamond detector response to the given doses of 1-400 cGy at depth of 1.5 cm for 6 MV photon beam, SSD = 100 cm.....	44
4.3 Variations of diamond detector sensitivity versus dose rate varied from 1.53–4.63 Gy/min for 6 MV photon beams, 10×10 cm <sup>2</sup> field size at depth of 1.5 cm.....	46
4.4 Variations of diamond detector response to the beam directions for 6 MV photon beams, measured free in air at isocenter.....	48
4.5 Output factors of 6 MV photon beam obtained by diamond detector, CC13 ionization chamber, and silicon diode detector, for field size of 10×10 cm <sup>2</sup> at depth of 1.5 cm, SSD = 100 cm.....	50
4.6 Depth dose curves of 10×10 cm <sup>2</sup> field size for 6 MV photon beams obtained by diamond detector, CC13 ionization chamber, and silicon diode detector.....	52
4.7 Depth dose curves of 4×4 cm <sup>2</sup> field size for 6 MV photon beams obtained by diamond detector, CC13 ionization chamber, and silicon diode detector.....	52



<b>Figure</b>	<b>Page</b>
4.8 Depth dose curves of $3 \times 3 \text{ cm}^2$ field size for 6 MV photon beams obtained by diamond detector, CC13 ionization chamber, and silicon diode detector.....	53
4.9 Depth dose curves of $2 \times 2 \text{ cm}^2$ field size for 6 MV photon beams obtained by diamond detector, CC13 ionization chamber, and silicon diode detector.....	53
4.10 Depth dose curves of $1.5 \times 1.5 \text{ cm}^2$ field size for 6 MV photon beams obtained by diamond detector, CC13 ionization chamber, and silicon diode detector.....	54
4.11 Beam profiles of $10 \times 10 \text{ cm}^2$ of 6 MV photon beams obtained by diamond detector, CC13 ionization chamber, and silicon diode detector.....	57
4.12 Beam profiles of $4 \times 4 \text{ cm}^2$ of 6 MV photon beams obtained by diamond detector, CC13 ionization chamber, and silicon diode detector.....	58
4.13 Beam profiles of $3 \times 3 \text{ cm}^2$ of 6 MV photon beams obtained by diamond detector, CC13 ionization chamber, and silicon diode detector.....	58
4.14 Beam profiles of $2 \times 2 \text{ cm}^2$ of 6 MV photon beams obtained by diamond detector, CC13 ionization chamber, and silicon diode detector.....	59
4.15 Beam profiles of $1.5 \times 1.5 \text{ cm}^2$ of 6 MV photon beams obtained by diamond detector, CC13 ionization chamber, and silicon diode detector.....	59

## LIST OF ABBREVIATIONS

<b>Abbreviation</b>	<b>Term</b>
3D	Three dimensions
A	Ampere
AAPM	The American Association of Physicists in Medicine
B <sup>+</sup>	Boron ion
C/Gy	Coulomb per gray
<sup>60</sup> Co	Cobalt 60
cc	Cubic centimeter
cc	Centiliter
CC13	Scanditronix/Wellhofer 0.13 cc ionization chamber
cGy	Centigray
cGy/min	Centigray per minute
cm	Centimeter
cm <sup>2</sup>	Square centimeter
CVD	Chemical vapor deposition
d <sub>max</sub>	Depth of maximum dose
e <sup>-</sup>	Electron
electrons/g	Electrons per gram
eV	Electronvolt
g/cm <sup>3</sup>	Gram per cubic centimeter
GPa	Gigapascal
Gy	Gray
Gy/min	Gray per minute
h <sup>+</sup>	Hole

<b>Abbreviation</b>	<b>Term</b>
IAEA	International Atomic Energy Agency
IMRT	Intensity Modulated Radiotherapy
kGy	Kilogray
LEDs	Light emitting diodes
MeV	Mega electronvolt
min	Minute
mm	Millimeter
mm <sup>2</sup>	Square millimeter
mm <sup>3</sup>	Cubic millimeter
MOSFET	Metal-oxide semiconductor field effect transistor
MU	Monitor unit
MU/min	Monitor unit per minute
MV	Megavolt
nC	Nanocoulomb
nC/Gy	Nanocoulomb per gray
nC/Gy mm <sup>3</sup>	Nanocoulomb per gray cubic millimeter
pC	Picocoulomb
PDD	Percentage depth dose
ps	Picosecond
QA	Quality assurance
RW <sub>50</sub>	Radiological width
SD	Standard deviation
SSD	Source surface distance
TPR <sup>20/10</sup>	Tissue phantom ratio of depth of 20 cm and 10 cm

<b>Abbreviation</b>	<b>Term</b>
TMR	Tissue maximum ratio
TRS	Technical report series
UV	Ultraviolet
V	Volt
VMAT	Volumetric Arc Therapy
Z	Atomic number
°	Degree
$\delta_1$	Delta 1
$\delta_2$	Delta 2
$\delta_3$	Delta 3
$\delta_{50-90}$	Beam fringe
$\mu\text{m}^3$	Cubic micromillimeter

สถาบันวิทยบริการ  
จุฬาลงกรณ์มหาวิทยาลัย



# CHAPTER I

## INTRODUCTION

### 1.1 Background and Rationale

In photon beam dosimetry, an ideal radiation detector should have the properties of high radiation sensitivity, high spatial resolution, constant response and soft tissue equivalent. The ionization chamber is often used in photon beam measurement. However, for the measurement in small photon beam or beam with steep dose gradients, ionization chamber has a drawback with low spatial resolution because of their large volume. In the other hand, if they have small volume, they will have low radiation sensitivity and non-uniform response. Thus, with small size and high sensitivity, the solid state detector is more suitable for using in such photon beams measurement. Silicon diode detector is widely and favorably used in radiotherapy field, nevertheless silicon has some drawbacks of beam energy dependence from its non-soft tissue equivalent ( $Z = 14$ ) properties. So diamond has been introduced for used as radiation detector, with atomic number  $Z = 6$  compared to  $Z = 7.4$  of soft tissue, diamond detector is suitable choice for the dosimetry of small photon beams or beams with steep dose gradients. [1-3]

PTW Riga natural diamond detector type 60003 is made from natural diamond crystal. Figure 1.1 shows this type of diamond detector. Many authors suggested to characterize each diamond detector because the diamond crystal used in each detector might have different impurity and present different behaviors in each detector. [2]



Figure 1.1 PTW Riga natural diamond detector type 60003.

Since the performance of diamond detector depends on its behaviors, Bucciolini *et al* [3] performed a study about the performance of diamond detector in photon beam by a diamond detectors belong to De Angelis *et al* [2] who studied about the characteristics of 2 diamond detectors. They reported the suitability of diamond

detector in photon beam dosimetry compared to those from a ionization chamber and a silicon diode. However, the smallest field size in their study was  $2.5 \times 2.5 \text{ cm}^2$  which is still large when compared to possible smallest field size used in sophisticated techniques such as intensity modulated radiotherapy.

The principle of radiation detection in diamond relies on the creation of electron-hole pairs within the diamond crystal from the interaction of the incident particles or photon. The local displacement of these carriers driven by an electronic field in the material induces a transient signal on the device electrodes. A typical configuration consists of applying an electric field through the volume of the diamond crystal in a sandwich configuration where electrical contacts are deposited on both sides. The electrodes are connected to an electrometer, to register a signal which is induced from interaction of the incident particles or photon in the diamond crystal.

This study aimed to investigate the characteristics of a diamond detector and evaluate its performance in small photon beam by compared to the performances of silicon diode and ionization chamber with field size down to  $1.5 \times 1.5 \text{ cm}^2$ , considered by the possible smallest field size that allow to use 0.13 cc ionization chamber.

## 1.2 Research Objectives

- 1.2.1 To investigate the characteristics of diamond detector in high energy photon beams.
- 1.2.2 To evaluate the performance of diamond detector in small photon beam.



สถาบันวิทยบริการ  
จุฬาลงกรณ์มหาวิทยาลัย

## CHAPTER II

### LITERATURE REVIEW

#### 2.1 Theories

##### 2.1.1 Radiation Detector [4]

Man possesses no biological sensors of ionizing radiation. As a consequence he must depend entirely on instrumentation for the detection and measurement of radiation. The basic requirement of any radiation-measuring instrument is that the instrument detector interacts with the radiation in such a manner that the magnitude of the instrument's response is proportional to the radiation effect or radiation property under measurement. Some of physical and chemical radiation effects that are applied for radiation detection and measurement are list in Table 2.1.

Table 2.1 Radiation effects used in the detection and measurement of radiation.

Effect	Type of Instrument	Detector
Electrical	1. Ionization chamber	1. Gas
	2. Proportional counter	2. Gas
	3. Geiger counter	3. Gas
	4. Solid state	4. Semiconductor
Chemical	1. Film	1. Photo graphic emulsion
	2. Chemical dosimeter	2. Solid or liquid
Light	1. Scintillation counter	1. Crystal or liquid
	2. Cerenkov counter	2. Crystal or liquid
Thermoluminescence	Thermoluminescence dosimeter	Crystal
Heat	Calorimeter	Solid or liquid

##### 2.1.2 Ionization Chamber [5]

The principle of the thimble chamber (or ionization chamber) is illustrated in Figure 2.1. In Figure 2.1A, a spherical volume of air is shown with an air cavity at the center. Suppose this sphere of air is irradiated uniformly with a photon beam. Also, suppose that the distance between the outer sphere and the inner cavity is equal to the maximum range of electron generated in air. If the number of electrons entering the cavity is the same as that leaving the cavity, electronic equilibrium exists. Suppose also that we are able to measure the ionization charge produced in the cavity by the electrons liberated in the air surrounding the cavity. Then by knowing the volume or mass of air inside the cavity, we can calculate the charge per unit mass or the beam exposure at the center of the cavity. Now if the air wall in Figure 2.1A is compressed into a solid shell as shown in Figure 2.1B, we get a thimble chamber as shown in Figure 2.1C. Although the thimble wall is solid, it is air equivalent, i.e. its effective

atomic number is the same as that of air. In addition, the thickness of the thimble wall is such that the electronic equilibrium occurs inside the cavity, just as it did in Figure 2.1A. As before, it follows that the wall thickness must be equal to or greater than the maximum range of the electrons liberated in the thimble wall.

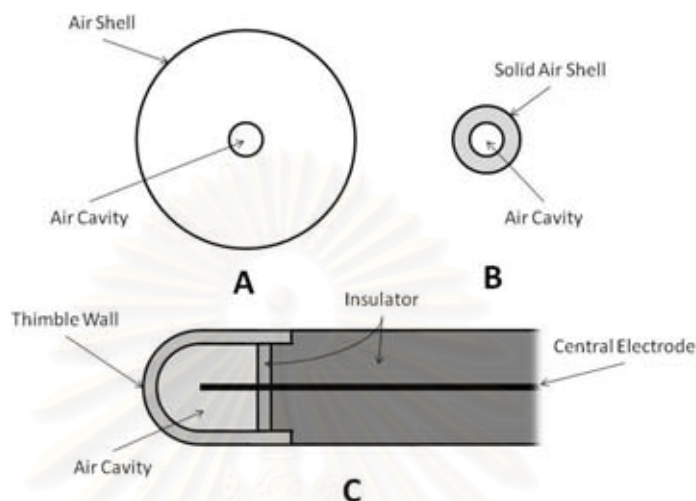


Figure 2.1 Schematic diagrams illustrating the nature of the thimble ionization chamber. (A) Air shell with air cavity. (B) Solid air shell with air cavity. (C) The thimble chamber.

Since the density of the solid air-equivalent wall is much greater than that of free air, the thickness required for electronic equilibrium in the thimble chamber are considerably reduced. For example, in the 100 to 250 kVp x-ray range, the wall thickness of the thimble (assuming unit density) is about 1 mm, and in the case of  $^{60}\text{Co}$   $\gamma$  rays (average  $h\nu \approx 1.25$  MeV), it is constructed with wall thickness of 1 mm or less and this is supplemented with close-fitting caps of Plexiglas or other plastic to bring the total wall thickness up to that needed for electronic equilibrium for the radiation in question.

#### *Desirable Chamber Characteristics*

A practical ion chamber for exposure measurement should have the following characteristic.

- 1) There should be minimal variation in sensitivity or exposure calibration factor over a wide range of photon energies.
- 2) There should be suitable volume to allow measurement for the expected range of exposures. The sensitivity (charge measurement per roentgen) is directly proportional to the chamber sensitivity volume. For example, the reading obtained for a given exposure with a  $30\text{ cm}^3$  chamber will be approximately 50 times higher than that obtained with a  $0.6\text{ cm}^3$  chamber. However, the ratio may not be exactly 50, since a chamber response also depends on the chamber design, as discussed earlier.
- 3) There should be minimal variation in sensitivity with the direction of incident radiation. Although this kind of variation can be minimized in the design of



the chamber, care is taken to use the chamber in the same configuration with respect to the beam as specified under chamber calibration conditions.

- 4) There should be minimal stem “leakage”. A chamber is known to have stem leakage if it records ionization produced anywhere other than its sensitive volume.
- 5) The chamber should have been calibrated for exposure against a standard instrument for all radiation qualities of interest
- 6) There should be minimal ion recombination losses. If the chamber voltage is not high enough or regions of low electronic field strength occur inside the chamber, such as in the vicinity of sharply concave surfaces or corners, ions may recombine before contributing to the measured charge. The problem becomes severe with high-intensity or pulsed beams.

Figure 2.2 shows basic circuit for an ionization chamber which has the electrical polarity. All the positive ions will be collected by the outer cathode, while the negative ions, or electrons, will be collected by the central anode.

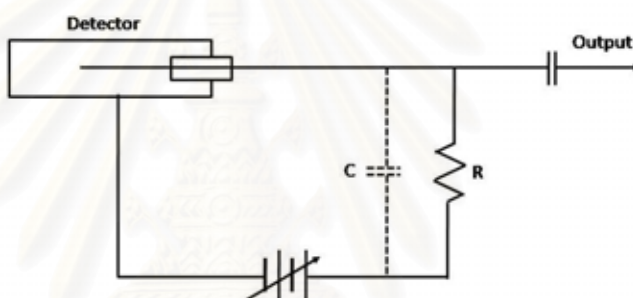


Figure 2.2 Basic circuits for an ionization chamber.

### 2.1.3 Semiconductor Detector [6-7]

A semiconductor detector is a device that uses a semiconductor material (usually silicon) to detect traversing charged particles or the absorption of photons. One of most interest for semiconductor using in dosimetry is their extremely high sensitivity relative to the ionization volume, the factor of about 18,000 is generally found between the response of a silicon diode and ionization chamber of the same volume. This allows reducing the sensitive volume to a few tenth of a cubic millimeter.

#### 2.1.3.1 Principle of Semiconductor

Figure 2.3 shows difference type of band structure, the semiconductor has small bandgap while insulator has large gap which not allow electron has sufficient energy to across the gap.

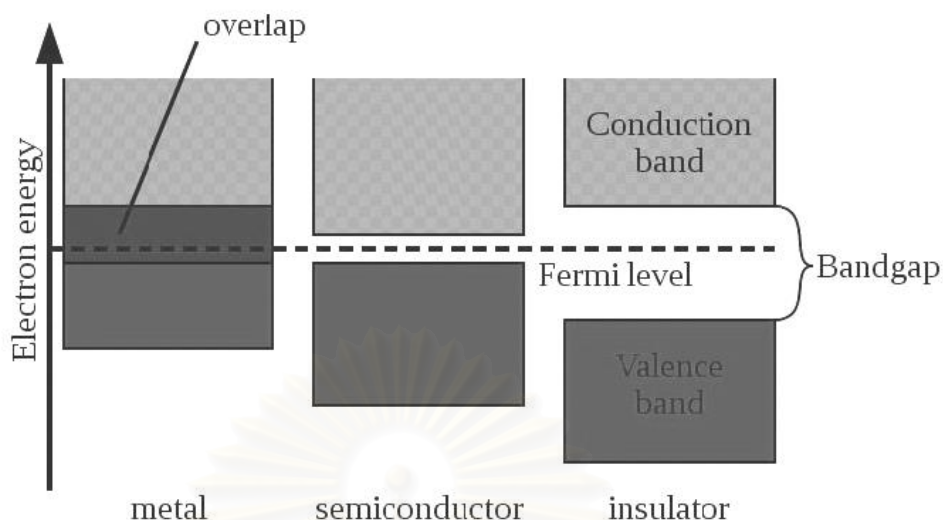


Figure 2.3 Difference type of band structure.

In the semiconductor radiation detectors, radiation is measured by means of the number of charge carriers set free in the detector, which is arranged between two electrodes. Ionizing radiation produces free electrons and holes. The number of electron-hole pairs is proportional to the energy transmitted by the radiation to the semiconductor. As a result, a number of electrons are transferred from the valence band to the conduction band, and an equal number of holes are created in the valence band. Under the influence of an electric field, electrons and holes travel to the electrodes, where they result in a pulse that can be measured in an outer circuit. The holes travel into the opposite direction and can also be measured. As the amount of energy required to create an electron-hole pair is known, and is independent of the energy of the incident radiation, measuring the number of electron-hole pairs allows the energy of the incident radiation to be found.

### 2.1.3.2 Type of Semiconductor

The semiconductor devices presently used for radiation dosimetry may be sorted into 2 types; silicon diodes and transistors. In addition, solid state ionization chamber made with silicon dioxide or diamond can be considered as semiconductor devices. Following the type of dosimetry, semiconductor devices can be used either as (a) electronic or real time dose rate-meters or (b) as solid state dosimeter.

- a) In the first case, the semiconductor device needs a bias voltage during operation. The involved dosimetric quantity corresponds to dose rate and is correlated with the produced electric current. Dose is obtained by integration.
- b) In the second case, the semiconductor device does not need any bias voltage. The dosimetric quantity corresponds to the absorbed dose and is correlated with the modification of a given physical parameter such as electric conductivity for the diode or threshold voltage. Mean dose rate can be obtained by means of sequential dose measurement.

### A. Silicon Diode Dosimeter

A silicon diode with an excess of electrons is called an  $n$ -type diode, while one with an equal number of electrons and holes. (These electrons and holes result from the rupture of the covalent bonds by absorption of heat or light energy.) By adding certain impurities to the crystal, either an excess number of electrons (an  $n$  region) or an excess number of holes (a  $p$  region) can be produced. Silicon is in group IV of the periodic table. If atoms from one of the elements in group V, such as phosphorus, arsenic, antimony, or bismuth, each of which has five valence electrons, are added to the pure silicon, four of the five electrons in each of the added atoms are shared by the silicon atom to form a covalent bond. The fifth electron from the impurity is thus an excess electron, and is free to move about in the crystal and to participate in the flow of electric current. Under these conditions, the crystal is of the  $n$  type. A  $p$ -type silicon diode, having an excess number of holes, can be made by adding an impurity from group III of the periodic table to the silicon crystal. Elements from group III, such as boron, aluminum, gallium, or indium, have three valence electrons. Incorporation of one of these elements as an impurity in the crystal, therefore, ties up only three of the four valence bonds in the crystal lattice. This deficiency of one electron is a hole, and we have  $p$ -type silicon diode.

Figure 2.4 shows the radiation detection principle of silicon diode which can be described by a  $p$  region in silicon that is adjacent to an  $n$  region is called an  $n$ - $p$  junction. If a forward bias is applied to the junction, that is, if a voltage is applied across the junction such that the  $p$  region is connected to the positive terminal and the  $n$  region to the negative terminal, the impedance across the junction will be very low, and current will flow across the junction. If the polarity of the applied voltage is reversed, that is, if the  $n$  region is connected to the positive terminal and the  $p$  region to the negative, we have the condition known as reverse bias. Under this condition, no current (except for a very small current due to thermally generated holes and electrons) flows across the junction. The region around the junction is swept free, by the potential difference, of the holes and the electrons in the  $p$  and  $n$  regions. This region is called the depletion layer, and is the sensitive volume of silicon diode. When an ionizing particle passes through the depletion layer, electron-hole pairs are

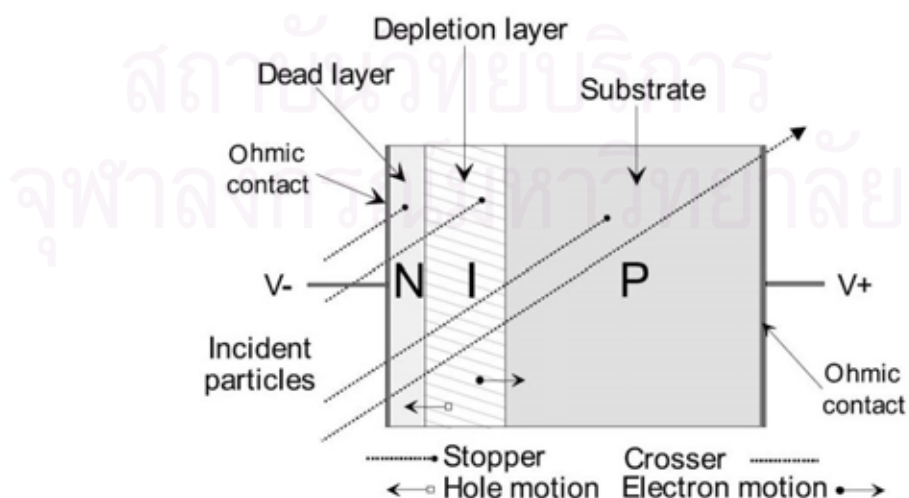


Figure 2.4 The radiation detection principle of silicon diode.

produced as a result of ionizing collisions between the ionizing particle and the crystal, the electric field then sweeps the holes and electrons apart, giving rise to a pulse in the load resistor as the electrons flow through the external circuit.

### B. Transistor Dosimeter

Transistor dosimeter mainly used for dosimetry is MOSFET (Metal-oxide semiconductor field effect transistor). By the name, MOSFET is field effect transistor where the channel size is controlled by the capacitance through an insulating material (silicon dioxide) in opposition to the classical field effect transistor where the channel size is controlled using a reverse junction. In a MOSFET no direct electric current can be injected from the gate. Generally the gate capacitance of a MOSFET is low and the gate power consumption strongly reduced. Such a transistor may be considered as a tap where the current flows from the source to the drain and the aperture of which is controlled by the voltage applied on the gate.

As an example the  $p$ -type MOSFET consist of a source and a drain, two highly conducting  $p$ -type semiconductor regions which are isolated from the  $n$ -type substrate by reverse biased  $p$ - $n$  diodes. A metallic (or polycrystalline) gate covers the region between the soured and the drain, but is separated from the semiconductor by the gate oxide. Figure 2.5 shows the schematic diagram of the MOSFET principle of an  $n$ -type MOSFET. Doping is made of  $B^+$ . The source and drain regions are identical. The applied voltage determines the  $p$ -type region from where electrons are derived and becomes the source, while the other  $p$ -type region collects the electrons and becomes the drain. The voltages apply to the drain and gate electrodes, as well as to the substrate by means of a back contact, are determined from the source potential.

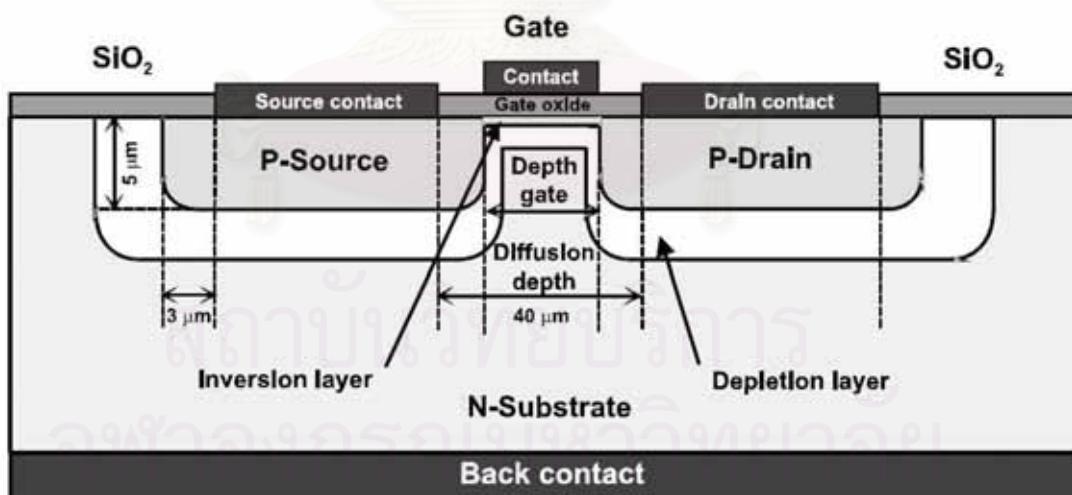


Figure 2.5 Diagram of the  $n$ -type MOSFET principle.



## 2.1.4 Diamond Detector

### 2.1.4.1 Diamond [8]

Diamond is transparent to opaque, optically isotropic, 3D-crystalline carbon. It is the hardest naturally occurring material known, owing to its strong covalent bonding, yet its toughness is only fair to good due to important structural weaknesses. The precise tensile strength of diamond is unknown. However, strength up to 60 GPa has been observed, and its theoretical intrinsic strength has been calculated to be between 90 and 225 GPa, depending on the crystal orientation. Diamond has a high refractive index (2.417) and moderate dispersion (0.044), properties which are considered carefully during diamond cutting and which (together with their hardness) give cut diamonds their brilliance and fire. Scientists classify diamonds into two main types and several subtypes, depending on the nature of crystallographic defects present. Trace impurities substitutionally replacing carbon atoms in a diamond's crystal lattice, and in some cases structural defects, are responsible for the wide range of colors seen in diamond. Most diamonds are electrical insulators but extremely efficient thermal conductors. The specific gravity of single-crystal diamond (3.52) is fairly constant. Contrary to a common misconception, diamond is not the most stable form of solid carbon; graphite has that distinction. Figure 2.6 shows structure lattice of diamond.

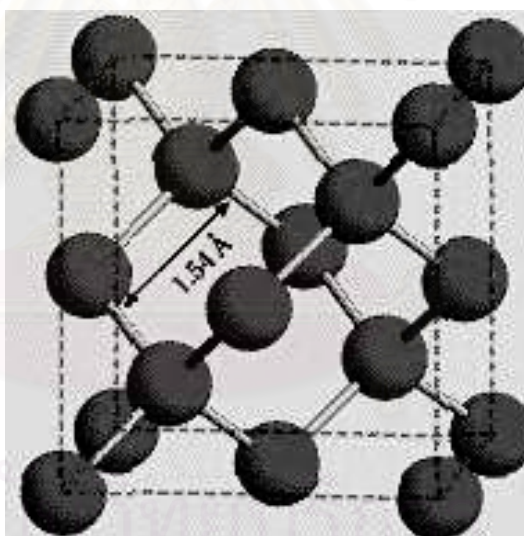


Figure 2.6 Structure of diamond crystal.

Except for most natural blue diamond which are semiconductors due to substitution of boron impurities replacing carbon atoms—diamond is a good electrical insulator. Natural blue or blue-gray diamonds, common for the Argyle diamond mine in Australia, are rich in hydrogen; these diamonds are not semiconductors and it is unclear whether hydrogen is actually responsible for their blue-gray color. Natural blue diamond containing boron and synthetic diamonds doped with boron are p-type semiconductors. N-type diamond films are reproducibly synthesized by phosphorus doping during chemical vapor deposition (CVD). Diode p-n junctions and UV light emitting diodes (LEDs, at 235 nm) has been produced by sequential deposition of p-type (boron-doped) and n-type (phosphorus-doped) layers



### 2.1.4.2 Diamond Detector [9]

The use of diamond in photoconductivity experiments began in 1923. Since then advances in the technology used to metalize the diamond at the edges to enable electrical contacts has promoted the use of diamond as a photoconducting detector of radiation. Extremely rapid turn-on and turn-off times ( $<100$  ps) have been demonstrated with the use of fast x-ray excitation of the diamond detectors. Diamond has a large band gap, radiation hardness, large saturated carrier velocity and low atomic number. This makes diamond a very attractive candidate as a radiation detector. Diamond can detect any radiation (UV, x-rays, gamma rays, charged particles, neutrons, pions and other high energy particles) that generates free carriers (electron-hole pairs) in the diamond. The fundamental mechanism of radiation detection in diamond is independent of the exciting radiation as long as it is more energetic than the band gap in diamond (5.5 eV).

A typical configuration consists of applying an electric field through the volume of the diamond layer in a sandwich configuration where electrical contacts are deposited on both sides. The electrodes are connected to an external voltage to provide an electric field across the device. Mobile charges produced as a result of absorbed radiation drift in this electric field and generate a current in the external circuit. Figure 2.7 Shows Diagram of the PTW diamond detector structure compare with its x-ray image.

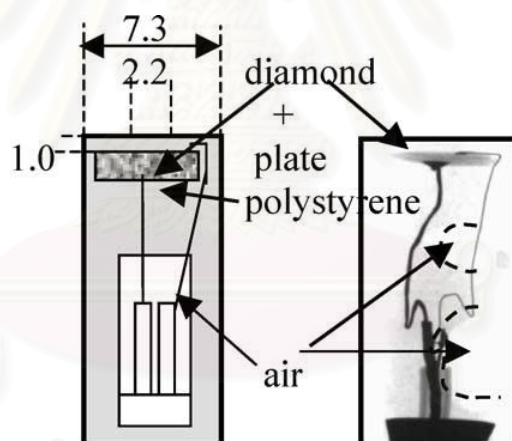


Figure 2.7 Diagram of the PTW diamond detector structure and its x-ray image. [10]

The use of natural diamond has been hindered by its rarity, very high cost and unpredictable electronic behavior due to lack of control of impurity content and crystal defects. Polycrystalline diamond promise to overcome these problems since it can be deposited by chemical vapour deposition (CVD) tuning the morphology (i.e. grain size and orientation) and electronic structure (i.e. intra-grain and grain boundary defects). In addition CVD diamond can be deposited on large area for image detection.

### 2.1.4.3 Comparison of Natural, CVD Diamond, Silicon Diode and MOSFET

Until recently the only form of diamond suitable for radiation detectors was natural diamond that constitutes a large fraction of the cost of the detectors. However, recent breakthroughs in chemical vapor deposition (CVD) processes have led to the production of economical, large CVD diamond wafers with electronic properties equal to or surpassing natural diamond. Table 2.2 shows comparison of material properties of nowadays available commercial semiconductor dosimeter i.e. natural diamond, CVD diamond, silicon diode and MOSFET.

**Table 2.2** Comparison of properties of natural diamond, CVD diamond, silicon diode, and MOSFET. [11]

Material characteristics	Natural diamond	CVD diamond	MOSFET	Silicon diode
Z number ( $Z_{\text{Tissue}} = 7.42$ )	6	6	14	14
Radiation damage	Negligible	Negligible	18 Gy	2% at kGy for <i>p</i> -type 7% at kGy for <i>n</i> -type
Toxicity	Non toxic	Non toxic	Non toxic	Non toxic
Temperature-dependence	Negligible	Negligible	<2%	0.4%/°C
Dosimetric geometry				
Sensitive volume	1-1.5 mm <sup>3</sup>	0.1 mm <sup>3</sup>	0.08 μm <sup>3</sup>	0.3 mm <sup>3</sup>
Field perturbation	Negligible	Negligible	Negligible	>7%
Angular dependence	Negligible	Negligible	2% at all angle	2% at 30° 5% at 60°
Metering characteristics				
Sensitivity	50-135 nC/Gy mm <sup>3</sup>	20 nC/Gy mm <sup>3</sup>	1-3 mV/cGy	200 nC/Gy mm <sup>3</sup>
Signal reproducibility	<0.5%	<1%	<3%	<0.5%
Energy dependence	Negligible	Negligible	<3%	Strongly dependence
Dose linearity range	0-13 Gy	0-10 Gy	0-25 Gy	0-10Gy
Dose rate-dependence	1-4%	6%	<3%	Strongly dependence

### 2.1.4.4 Polarization Effect [12]

The passage of radiation through the diamond produces the excitation of electrons from valence to conduction band, and these electrons can be subsequently captured in active traps inside the forbidden gap, deep traps get progressively trapped and end up filled throughout the entire device. After being filled, they are supposed to be stable and not perturbing the response. However, shallow traps are progressively emptied due to thermal agitation. Therefore, the probability to be refilled is greater in the region where more electrons circulate, thus e.g. for electrons closer to the anode side. This implies the existence of a charge of negative sign on the anode side, that builds up during use of the device, and that vanishes progressively when irradiation is stopped. This negative charge lowers the overall electric field, thus is responsible for the decrease in sensitivity. Similarly, the same illustration can be made for holes, on other deep and shallow traps, and resulting in the buildup during use of a charge of positive sign on the anode side, also resulting in lower sensitivity. Figure 2.8 shows illustration of polarization effect.

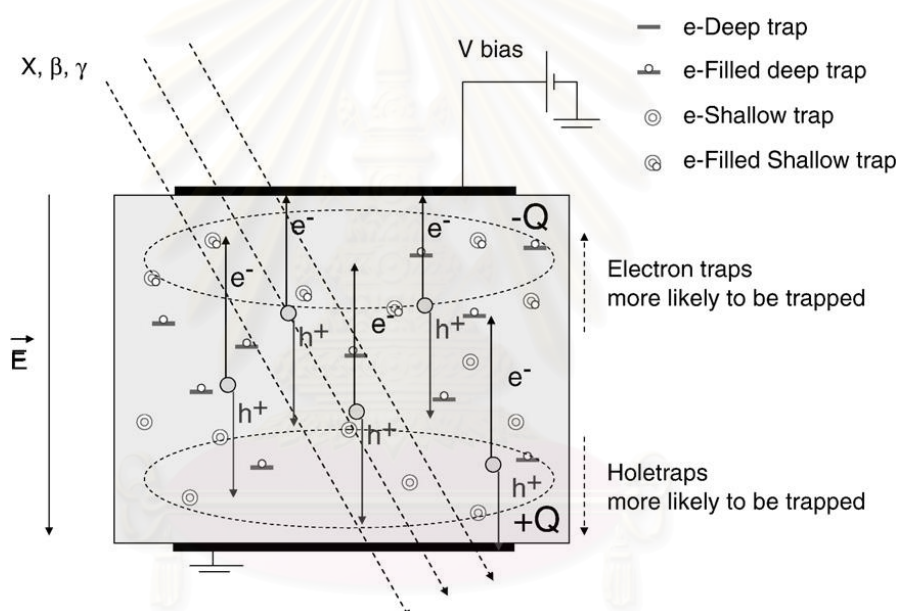


Figure 2.8 Illustration of polarization effect.

## 2.1.5 Dose Distribution, Beam Output and Beam Profile. [5]

### 2.1.5.1 Depth Dose Distribution

As the beam is incident on a patient (or a phantom), the absorbed dose in the patient varies with depth. This variation depends on many conditions: beam energy, depth, field size, distance from source, and beam collimation system. Thus the calculation of dose in the patient involves considerations in regard to these parameters and others as they affect depth dose distribution.

An essential step in the dose calculation system is to establish depth dose variation along the central axis of the beam. A number of quantities have been defined for this purpose, major among these being percentage depth dose, tissue-air ratios,

tissue-phantom ratios, and tissue-maximum ratios. These quantities are usually derived measurement made in water phantom using small ionization chamber. Although other dosimetry system such as TLD, diodes, and film are occasionally used, ion chamber are preferred because of their better precision and smaller energy dependence.

### 2.1.5.2 Percentage Depth Dose

One way of characterizing the central axis dose distribution is to normalize dose at depth with respect to dose at a reference depth. The quantity *percentage* (or simply *percent*) *depth dose* may be defined as the quotient, expressed as a percentage, of the absorbed dose at any depth  $d$  to the absorbed dose at affixed reference depth  $d_0$ , along the central axis of the beam (Figure 2.9). Percentage depth dose ( $P$ ) is thus

$$P = \frac{D_d}{D_{d_0}} \times 100$$

For orthovoltage (up to about 400 kVp) and lower-energy x-rays, the reference depth is usually the surface ( $d_0 = 0$ ). For higher energies, the reference depth is taken at the position of the *peak absorbed dose* ( $d_0 = d_m$ ).

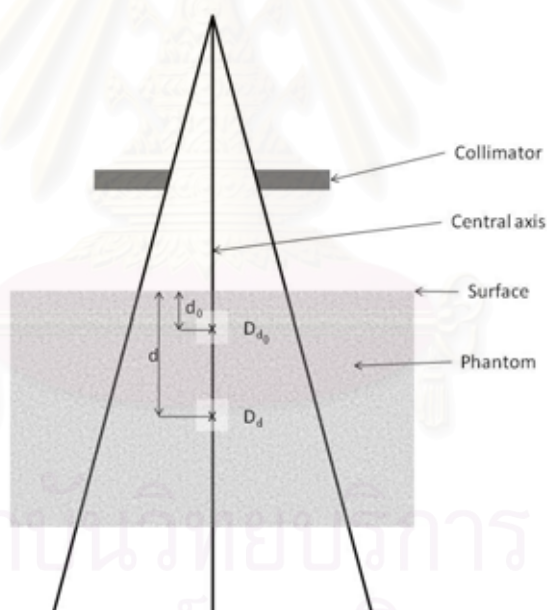


Figure 2.9 Percentage depth dose is  $(D_d/D_{d_0}) \times 100$ , where  $d$  is any depth and  $d_0$  is reference depth of maximum dose.

In clinical practice, the peak absorbed dose on the central axis is sometimes called the *maximum dose*, the *dose maximum*, the *given dose*, or simply the  $d_{max}$ . Thus

$$D_{max} = \frac{D_d}{P} \times 100$$

A number of parameters affect the central axis depth dose distribution. These include beam quality or energy, depth, field size and shape, source to surface distance, and beam collimation. A discussion of these parameters will now be presented.

#### A. Dependence on Beam Quality and Depth

The percentage depth dose (beyond the depth of maximum dose) increases with beam energy. Higher-energy beams have greater penetrating power and thus deliver a higher percentage depth dose (Figure 2.10). If the effects of inverse square law and scattering are not considered, the percentage depth dose variation with depth is governed approximately by exponential. Thus the beam quality affects the percentage depth dose by virtue of the average attenuation coefficient. As the beam energy increases, the more penetrating the beam becomes, resulting in a higher percentage depth dose at any given depth beyond the build-up region.

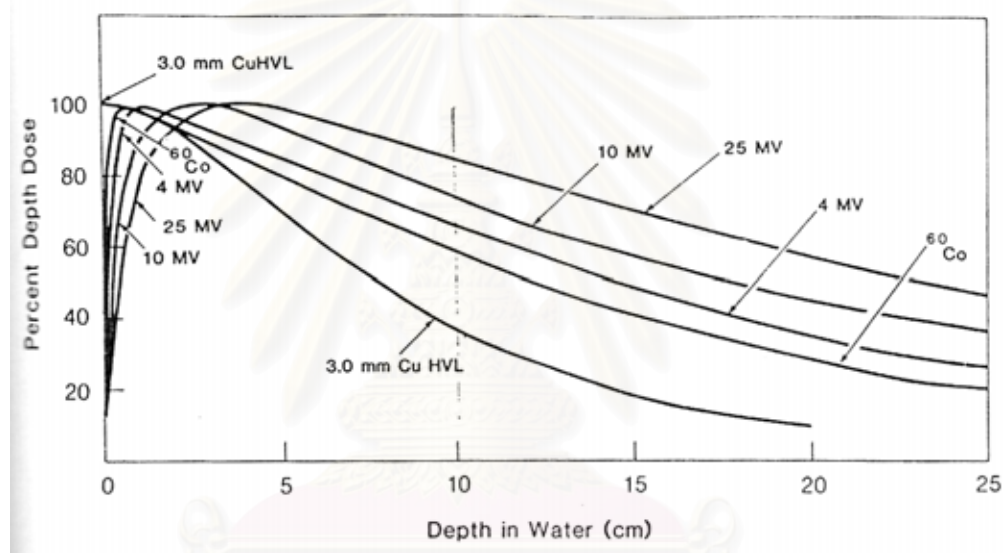


Figure 2.10 Central axis depth dose distribution for different quality photon beams. Field size  $10 \times 10 \text{ cm}^2$ ; SSD = 100 cm for all beams except for 3.0 mm Cu HVL, SSD = 50 cm.

#### *Initial Dose Buildup*

As seen in Figure 2.10, the percentage depth dose decreases with depth beyond the depth of maximum dose. However, there is an initial buildup of dose which becomes more and more pronounced as the energy is increased. In the case of the orthovoltage or lower-energy x-rays, the dose builds up to a maximum on or very close to the surface. But for higher energy beams, the point of maximum dose lies deeper into the tissue or phantom. The region between the surface and the point of maximum dose is called the *dose build up region*.

The physics of dose buildup may be explained as follows. (a) As the high energy photon beam enters the patient or the phantom, high speed electrons are ejected from the surface and the subsequent layers. (b) These electrons deposit their energy a significant way from their side of origin. (c) Because of (a) and (b), the



electron fluence and hence the absorbed dose increase with depth until they reach a maximum. However, the photon energy fluence continuously decreases with depth and, as a result, the production of electrons also decreases with depth. The net effect is that beyond a certain depth the dose eventually begins to decrease with depth.

It may be instructive to explain the buildup phenomenon in terms of absorbed dose and a quantity known as kerma (from kinetic energy released in the medium). The kerma may ( $K$ ) be defined as “the quotient of  $dE_{tr}$  by  $dm$ , where  $dE_{tr}$  is the sum of the initial kinetic energies of all the charged ionizing particles (electrons) liberated by uncharged ionizing particles (photons) in a material of mass  $dm$ ”.

$$K = \frac{dE_{tr}}{dm}$$

Since kerma represents the energy transferred from photons to directly ionizing electrons, the kerma is maximum at the surface and decreases with depth because of the decrease of the photon energy fluence (Figure 2.10). The absorbed dose, on the other hand, first increases with depth as the high speed electrons ejected at various depths travel downstream. As a result, There is an electronic buildup with depth. However, as the dose depends on electron fluence. It reaches a maximum at a depth approximately equal to the range of electrons in the medium. Beyond this depth, the dose decreases as kerma continues to decrease, resulting in a decrease in secondary electron production and hence a net decrease in electron fluence. As seen in figure 2.11, the kerma curve is initially higher than the dose curve but falls below the dose curve beyond the buildup region. This effect is explained by the fact that the areas under the two curves taken to infinity must be the same.

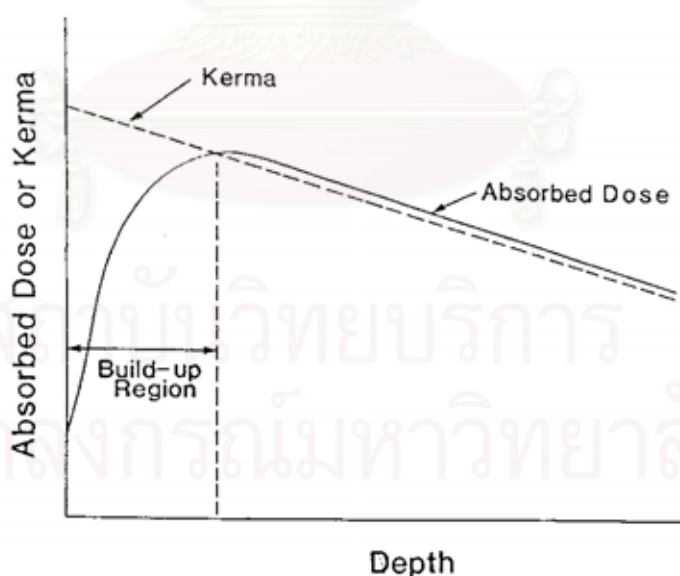


Figure 2.11 Schematic plot of absorbed dose and kerma as functions of depth.

## B. Effect of Field Size and Shape

Field size may be specified either geometrically or dosimetrically. The geometrical field size is defined as “the projection, on a plane perpendicular to the beam axis, of the distal end of the collimator as seen from the front center of the source”. This definition usually corresponds to the field defined by the light localizer, arranged as if a point source of light were located at the center of the front surface of the radiation source. The dosimetric, or physical, field size is the distance intercepted by a given isodose curve (usually 50% isodose) on a plane perpendicular to the beam axis at a started distance from the source.

In addition, the field size will be defined at a predetermined distance such as the *source-surface distance* (SSD) or the *source-axis distance* (SAD). The latter term is the distance from the source to axis of gantry rotation known as the *isocenter*.

For a sufficiently small field one may assume that the depth dose at a point is effectively the result of the primary radiation, i.e., the photons which have traversed the overlying medium without interacting. The contribution of scattered photons to the depth dose in this case is negligibly or small or 0. But as the field size is increased, the contribution of the scattered radiation to the absorbed dose increases. Since this increase in scattered dose is greater in larger depth than at the depth of  $D_{\max}$ , the percent depth dose increases with increasing field size.

The increase in percentage depth dose caused by increase in field size depends on beam quality. Since the scattering probability or cross-section decreases with energy increase and the higher-energy photons are scattered more predominantly in the forward direction, the field size dependence of percent depth dose is less pronounced for the higher energy than for the low-energy beam.

## C. Dependence on Source-Surface Distance

Photon fluence emitted by a point source of radiation varies inversely as a square of the distance from the source. Although the clinical source (isotropic source or focal spot) for external beam therapy has a finite size, the source-surface distance is usually chosen to be large ( $\geq 80$  cm) so that the source dimensions becomes unimportant in relative to the variation of photon fluence with distance. In other words, the source can be considered as a point at large source-surface distance. Thus the exposure rate or “dose rate in free space” from such a source varies inversely as the square of the distance. Of course, the inverse square law dependence of dose rate assumes that we are dealing with a primary beam, without scatter. In a given clinical situation, however, collimation or other scattering material in the beam may cause deviation from the inverse square law.

Percent depth dose increases with SSD because of the effects of the inverse square law. Although the actual dose rate at a point decreases with increases in distance from the source, the percent depth dose, which is a relative dose with respect to a reference point, increases with SSD. This is illustrated in Figure 2.12 in which relative dose rate from a point source of radiation is plotted as a function of distance from the source, following the inverse square law. The plot shows that the drop in dose rate between two points is much greater at smaller distance from the source than at large distance. This means that the percent depth dose, which represents depth dose

relative to a reference point, decreases more rapidly near the source than far away from the source.

In clinical radiotherapy, SSD is a very importance parameter. Since percent depth dose determines how much dose can be delivered at depth relative to the surface dose or  $D_{\max}$ , the SSD needs to be as large as possible. However, since dose rate decreases with distance, the SSD, in practice, is set at a distance which provides a compromise between dose rate and percent depth dose. For treatment of deep-seated lesions with megavoltage beams, the minimum recommended SSD is 80 cm.

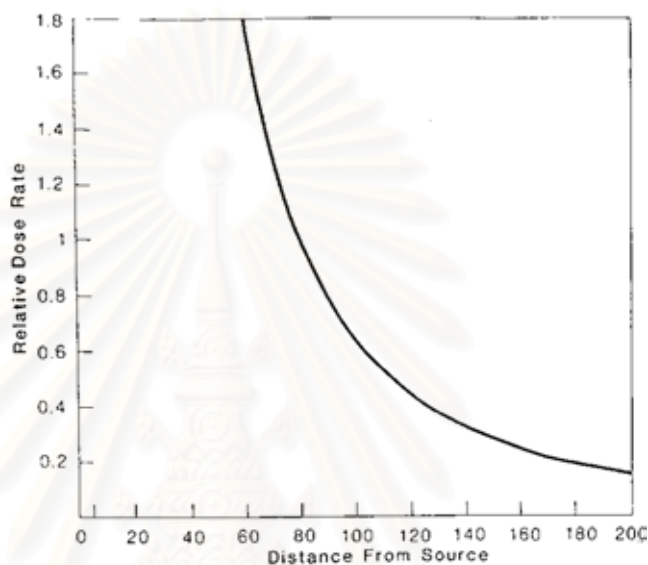


Figure 2.12 Plot of relative dose rate as inverse square law function of distance from a point source. Reference distance = 80 cm.

### 2.1.5.3 Beam Output

The beam output (exposure rate, dose rate in free space, or energy fluence rate) measure in air depends on the field size. As the field size is increased, the output increases because of the increased collimator scatter which is added to the primary beam.

The *collimator scatter factor* ( $S_c$ ) is commonly called the *output factor* and may be defined as the ratio of the output in air for a given field to that for a reference field (e.g.,  $10 \times 10 \text{ cm}^2$ ).  $S_c$  may be measure with an ion chamber with a build up cap of a size enough to provide maximum dose buildup for the given energy beam. The measurement setup is shown in Figure 2.13A. Readings are plotted against field size [side of equivalent square or area/perimeter (A/P)] and the values are normalized to the reference field ( $10 \times 10 \text{ cm}^2$ ).

In the measurement of  $S_c$ , the field must fully cover the build-up cap for all field size if measurements are to reflect relative photon fluence. For small fields, one may take the measurements at large distance from the source so that the smallest field covers build-up cap. Normally, the collimator scatter factors are measured at the

source-axis distance (SAD). However, larger distance can be used provided the field sizes are all defined at the SAD.

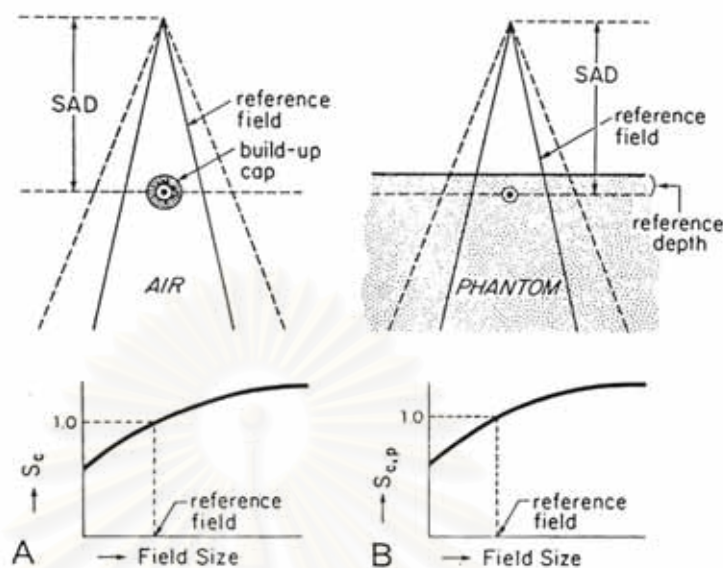


Figure 2.13 Arrangement for measuring (A)  $S_c$  and (B)  $S_{c,p}$ .

The *phantom scatter factor* ( $S_p$ ) takes into account the change in scatter radiation originating in the phantom at a reference depth as the field size is changed.  $S_p$  may be defined as the ratio of the dose rate for a given field at a reference depth (e.g., depth of maximum dose) to the dose rate at the same depth for the reference field size (e.g.,  $10 \times 10 \text{ cm}^2$ ), with the same collimator opening. Thus one could determine  $S_p$ , at least in concept, by using a large field incident on phantom of various cross-sectional sizes.

For photon beams for which backscatter factors can be accurately measured (e.g.,  $\text{Co}^{60}$  and 4 MV),  $S_p$  factor at the depth of maximum dose may be defined simply as the ratio of backscatter factor (BSF) for the given field to that for the reference field. Mathematically,

$$S_p(r) = \frac{BSF(r)}{BSF(r_0)}$$

where  $r_0$  is the side of the reference field size ( $10 \times 10 \text{ cm}^2$ ).

A more practical method of measuring  $S_p$ , which can be used for all beam energies, consists of indirect determination from the following equation,

$$S_p(r) = \frac{S_{c,p}(r)}{S_c(r)}$$

Where  $S_{c,p}(r)$  is the total scatter factor defined as the dose rate at a reference depth for a given field size  $r$  divided by the dose rate at the same point and depth for the reference field size ( $10 \times 10 \text{ cm}^2$ ) (see Figure 2.13B). Thus  $S_{c,p}(r)$  contains both the scatter and phantom scatter and when divided by  $S_c(r)$  yields  $S_p(r)$ .



Since  $S_p$  and  $S_{c,p}$  are defined at the reference depth of  $D_{max}$ , actual measurement of these factors at this depth may create problems because of the possible influence of contaminant electrons incident on the phantom. This can be avoided by making measurement at greater depth (e.g. 10 cm) and converting the readings to the reference depth of  $D_{max}$  by using percent depth dose data, presumably measured with a small-diameter chamber. The rationale for this procedure is the same as for the recommended depths of calibration.

#### 2.1.5.4 Beam Profile

The representation of the beam which shows the dose variation across the field at a specified depth is known as the *beam profile*. It may be noted that the field size is defined as the lateral distance between the 50% isodose lines at a reference depth. This definition is practically achieved by a procedure called the beam alignment in which the field-defining light is made to coincide with the 50% isodose lines of the radiation beam projected on a plane perpendicular to the beam axis and at the standard SSD or SAD.

Another way of depicting the dose variation across the field is to plot isodose curves in a plane perpendicular to the central axis of the beam. Such a representation is useful for treatment planning in which the field sizes are determined on basis of an isodose curve (e.g., 90%) that adequately covers the target volume.

Examination of beam profile reveals some general properties of dose distribution of beam.

- 1) The dose at any depth is greatest on the central axis of the beam and gradually decreases toward the edges of the beam, with the exception of some linac x-ray beams which exhibit areas of high dose or "horns" near the surface in the periphery of the field. These horns are created by the flattening filter which is usually designed to overcompensate near the surface in order to obtain flat isodose curves at greater depths.
- 2) Near the edges of the beam (the penumbra region), the dose rate decreases rapidly as a function of lateral distance from the beam axis. The width of geometric penumbra which exists both inside and outside the geometrical boundaries of the beam, depends on source size, distance from source, and source-to-diaphragm distance.
- 3) Near the beam edge, falloff of the beam is caused not only by the geometric penumbra but also by the reduced side scatter. Therefore, the geometric penumbra is not the best measure of beam sharpness near the edges. Instead the term *physical penumbra* may be used. The physical penumbra width is defined as the lateral distance between two specified isodose curves at a specified depth (e.g., lateral distance between 90% and 20% isodose line at depth of  $D_{max}$ ).
- 4) Outside the geometric limits of the beam and the penumbra, the dose variation is the result of side scatter from the field and both leakage and scatter from the collimator system. Beyond this collimator zone, the dose distribution is governed by the lateral scatter from the medium and leakage from the head of the machine (often called *therapeutic housing* or *source housing*)



## 2.2 Related literature Review

De Angelis et al [2] studied the operating characteristics between two PTW Riga diamond detectors. They investigated in the polarization effect, current-voltage characteristics, time stability, absorbed dose response, dose rate dependence, temperature stability, directional dependence of response and beam quality dependence of sensitivity. They reported differences of some parameters between the diamond detectors and showed that diamond detector behaviors were individual for each detector. Moreover, they reported the difference between exact appropriated value of operating parameter from their study and what stated in PTW Measuring Probe Certificate i.e. pre-irradiation doses which depend on polarization effect. They found pre-irradiation suggested in the certificated was less than 10 Gy but it was not enough to stabilize the detector response which required the dose of 15 Gy. They also suggested the characterization of each diamond detector according to its individual behavior because the PTW diamond detector made from natural growth diamond crystals that might present different concentration of impurity and defect. Thus, there was not only pre-irradiation dose that was difference but also the other characteristics which due to the concentration of defect which indicated to the response of the detector both directly and indirectly. Beside pre-irradiation dose, they also reported dependence on dose rate which required fitting parameter for correction and also stated in PTW Measuring Probe Certificate but only indicative and must be experimentally determination.

Bucciolini M et al [3] studied the performance of diamond detector in small photon beam compared with a ionization chamber and silicon diode. They used a diamond detector used in study of De Angelis et al. and this diamond detector was better than another detector. They performed measurement of output factors, depth dose curves and beam profiles. The field sizes were  $10 \times 10$ ,  $5 \times 5$ , and  $2.5 \times 2.5$  cm<sup>2</sup> so it was smallest field size in the study. The output factors in 25 MV photon beams obtained by diamond detector were higher than those obtained by ionization chamber and silicon diode in all field size studied while lowest in  $5 \times 5$  cm<sup>2</sup> field size of 6 MV. For the percentage depth dose measurement, PDD by diamond detector have good agreement with the others except in distal depth with silicon diode which has energy dependent and overestimated in 6 MV photon beam but fewer overestimated in 25MV beam. For beam profile measurements, ionization chamber was reported that was not a suitable detector when high spatial resolution is required. The penumbras determined by ionization chamber were higher than other in all field size. Since they were measured within steep dose gradient, the volume effect was pronounced. In this study, diamond detector was seem the best choice for these dosimetric application.

Rustgi S N [1] published some characteristics of diamond detector and its performance in term of spatial resolution and determination of tissue maximum ratio (TMR). For the characteristics, Rustgi performed study for investigated the diamond sensitivity, tissue equivalence and directional dependence compared to silicon diode in cobalt60, 6MV photon and 18MV photon beams. Rustgi reported almost uniform sensitivity and nearly tissue equivalence of diamond detector with slightly directional dependence in photon beam at angle larger than  $135^\circ$ . For the spatial resolution, compared with a 0.14cc ionization chamber and a silicon diode, diamond detector was slightly inferior to silicon diode but much superior to that of small volume ionization

chamber. For determination of TMR, compared with a Markus parallel plate chamber and a silicon diode, there were comparable with agreement better than  $\pm 1\%$ .

Rustgi et al [13] reported the performance of diamond detector, ionization chamber, Markus parallel plate chamber, silicon diode and Kodak XV-2 ready pack film. Total scatter factor or output factor and TMR were determined for circular field size which varied from diameter 1.25-40 mm in 2.5 mm steps for 6 MV photon beam by using diamond detector, Markus parallel plate chamber, and silicon diode. The output obtained by diamond and diode were comparable, nevertheless those by diamond detector were slightly lower because its sensitive volume was slightly larger than diode. For output obtained by Markut, with large size, they were underestimated. For TMR, There were in agreement within  $\pm 1\%$  and effect of diode from silicon to low energy was not observed because the diode was energy compensated. For beam profiles measurement, diamond detector, ionization chamber, silicon diode and Kodak XV-2 ready pack film were used for comparison. Diamond, silicon diode and film were comparable while larger penumbras were determined by ionization chamber.



สถาบันวิทยบริการ  
จุฬาลงกรณ์มหาวิทยาลัย

# CHAPTER III

## RESEARCH METHODOLOGY

### 3.1. Research Design

This study is an observational research descriptive study.

### 3.2. Research Design Model

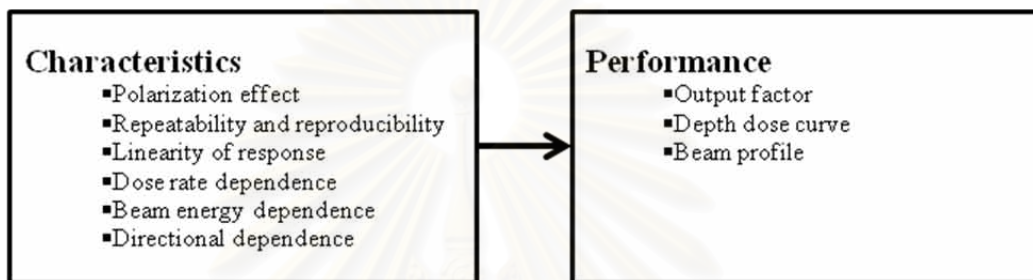


Figure 3.1 Research design model.

### 3.3. Conceptual Frameworks

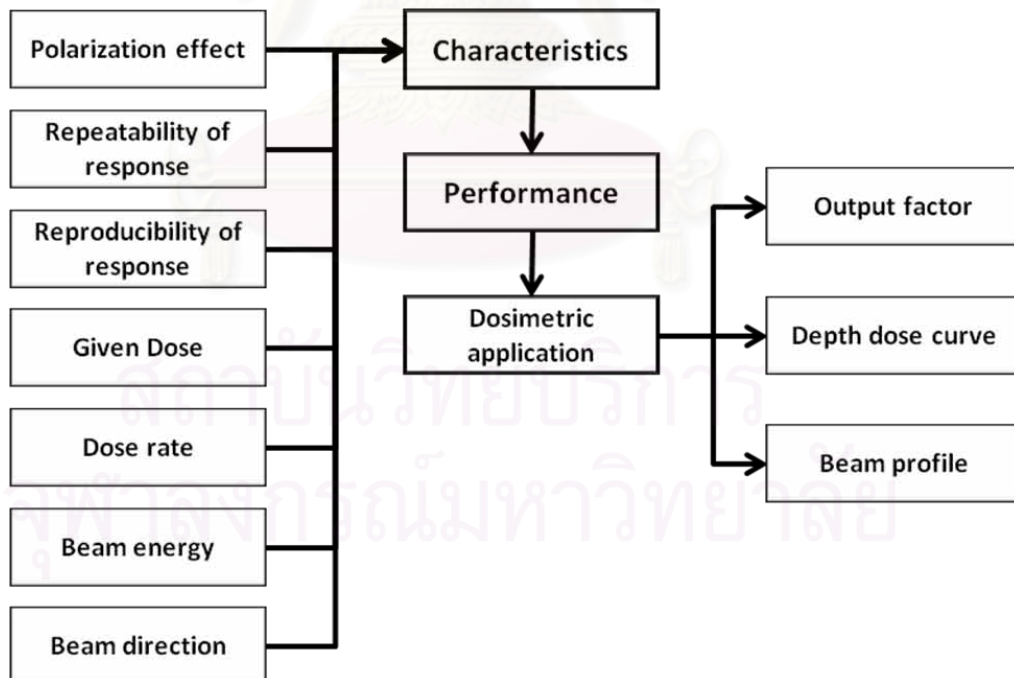


Figure 3.2 Conceptual frameworks.

### 3.4. Key Words

- Diamond Detector
- Small Photon Beam
- Dosimetry
- Small Field Measurement

### 3.5. Materials

#### 3.5.1. Diamond Detector

PTW Riga natural diamond detector type 60003, manufactured by PTW Freiberg, Germany, was used. Figure 3.3 shows the diagram of this type of diamond detector and Table 3.1 reports its physical and operating parameters which are in the PTW Diamond Detector Type 60003 User Manual. [14]

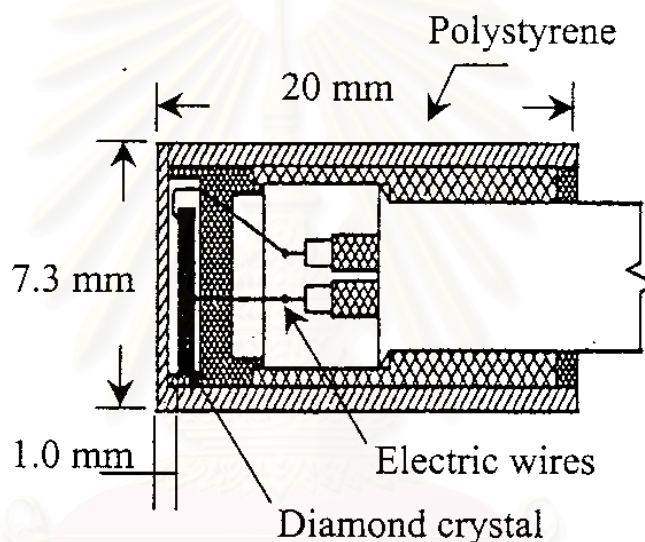


Figure 3.3 Diagram of the diamond detector. [1]

Table 3.1 Physical and operating parameters of the PTW diamond detector.

Manufacture	PTW Freiberg, Germany
Serial number	4-015
Sensitive volume	1.2 mm <sup>3</sup>
Sensitive area	4.3 mm <sup>2</sup>
Thickness of sensitive volume	0.28 mm.
Pre irradiation dose	<10 Gy
Operating bias	(+100 ±0.1) V
Dark current	5x10 <sup>-13</sup> A
Detector sensitivity to Co <sup>60</sup> at depth of 5 cm, field size of 10 x 10 cm <sup>2</sup> , SSD 75 cm.	1.00 x 10 <sup>-7</sup> C/Gy

### 3.5.2.Linear Accelerator

Figure 3.4 shows the Varian Clinac 21 EX which is the linear accelerator (or linac) used in this study. The machine was installed in 2004 at Division of Radiation Oncology, Department of Radiology, King Chulalongkorn Memorial Hospital. It can provide photon beams of 6 and 10 MV and electron beams of 6, 9, 12, 16, and 20 MeV. This machine is equipped with multileaf collimators which has collimator width of 1 cm. The QA for the machine was performed for daily, weekly, monthly and yearly according to AAPM report no.46. [15]

In this study, 6 MV photon beams were employed for the characteristic and performance studies, the 10 MV photon beams were used for energy dependent study. The beam quality was characterized by a  $TPR^{20}_{10}$  of 0.668 and 0.738 for 6 and 10 MV, respectively. The field size of  $10 \times 10 \text{ cm}^2$  was used as a reference field size. For diamond detector performance, the small field sizes used were  $4 \times 4$ ,  $3 \times 3$ ,  $2 \times 2$  and  $1.5 \times 1.5 \text{ cm}^2$ .



Figure 3.4 Linear accelerator (Varian Clinac 21 EX).



### 3.5.3. Phantom

#### 3.5.3.1. Solid Water Phantom

Figure 3.5 shows solid water phantom made from epoxy resin based mixture which has similar mass density and electron density to water ( $1.00\text{g/cm}^3$  and  $3.34 \times 10^{23}$  electrons/g, respectively). A set of solid water phantom in this study was consisted of  $30 \times 30 \text{ cm}^2$  solid water phantom of various thicknesses and solid water phantom slabs which have a cavity fit for insert the specific detector.



Figure 3.5 Solid water phantoms.

#### 3.5.3.2. Beam Scanner Water Phantom

Figure 3.6 shows the Blue phantom, manufactured by Scanditronix/Wellhofer, is an advanced 3D water phantom system for commissioning and QA of linac. It has high positioning accuracy control which is operated through the OmniPro-Accept software.

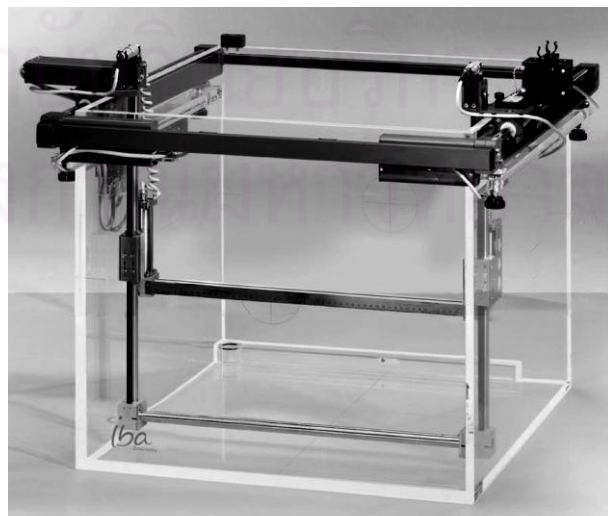


Figure 3.6 Blue phantom.

### 3.5.4. Electrometer

Dose1 electrometer, manufactured by Scanditronix/Wellhofer, can measure electrical charge in the range of 40 pC to 1.0 C at 0.1 pC resolution. Its display can report the measurement values with clearly digital number. The dose1 electrometer can connect with the diamond detector with an adaptor cable. Figure 3.7 shows Dose1 electrometer.



Figure 3.7 Dose1 electrometer.

### 3.5.5. Adapter Cable

Figure 3.8 shows the adapter cable, manufactured by PTW Freiburg, Germany which is the same manufacturer with the diamond detector.



Figure 3.8 PTW adapter cable.

### 3.5.6. Ionization Chamber

Scanditronix/Wellhofer 0.13 cc ionization chamber or CC13 was employed for comparing the dosimetric performance with the diamond detector. Its cavity diameter, cavity length, and sensitive volume are 4 mm, 10 mm, and 0.13 cc, respectively. Figure 3.9 shows the CC13 compared its size with diamond detector and silicon diode.

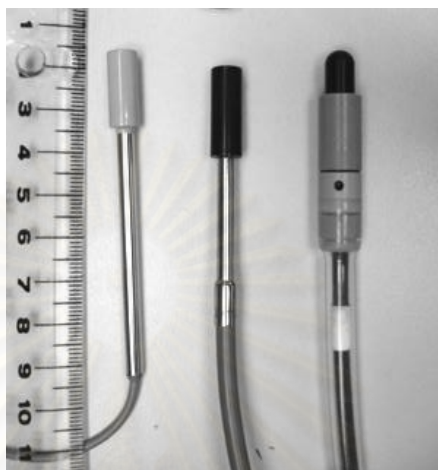


Figure 3.9 The detectors used in this study  
(Left: Silicon diode, Middle: Diamond detector, Right: CC13).

### 3.5.7. Silicon Diode Detector

Scanditronix/Wellhofer *p*-type silicon diode detector was employed for comparing the dosimetric performance with the diamond detector. Its diameter, sensitive volume, and sensitive volume thickness are 2.5 mm,  $3 \times 10^{-3}$  cc, and 60  $\mu\text{m}$ , respectively. Figure 3.9 shows the Silicon diode compare its size with diamond detector and CC13 ionization chamber.

### 3.5.8. Build Up Cap

A build up cap made from paraffin wax was used in beam directional dependence. Figure 3.10 shows the build up cap of 4.6 cm diameter with a fitted hole for diamond detector.

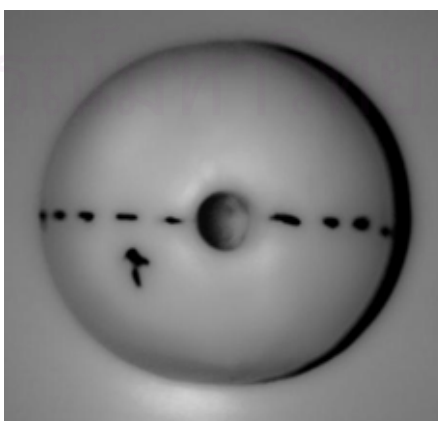


Figure 3.10 Build up cap

### 3.6. Methods

#### 3.6.1. Characteristics of Diamond Detector

##### 3.6.1.1. Setup of Measurement

Figure 3.11 shows a diagram of diamond detector and phantom setup used as typical setup in the study of characteristics of diamond detector. This setup was used throughout the characteristics studies unless there was referred to use other specified setup for that study.

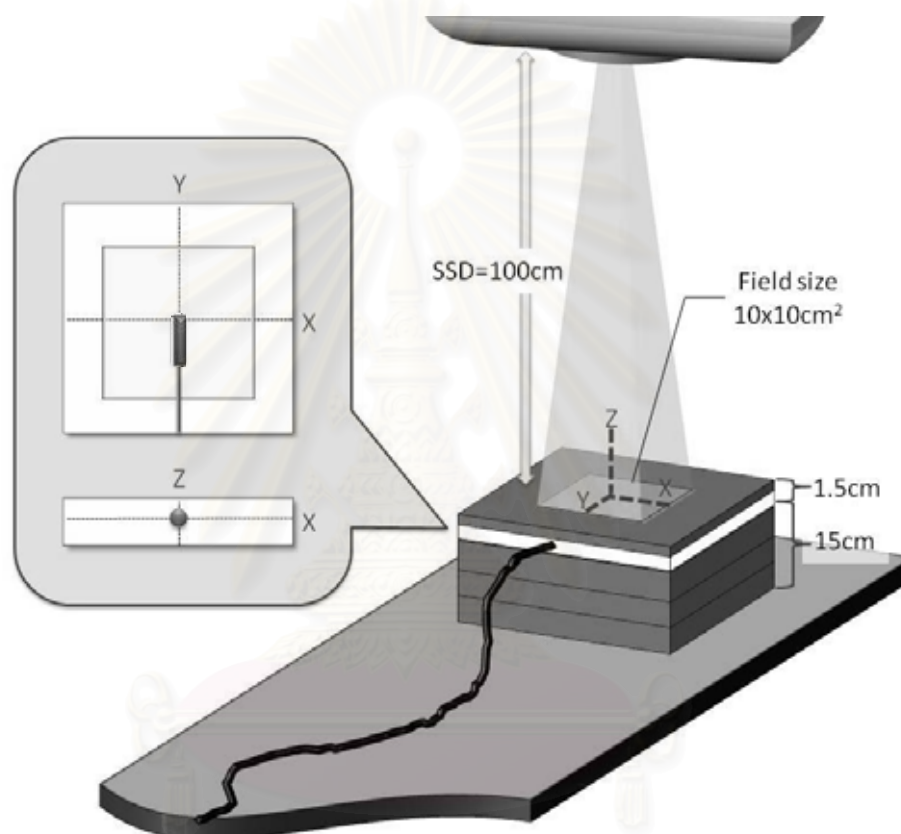


Figure 3.11 Diagram of typical set-up in characteristics studies.

#### *Procedure*

- 1) Solid water phantom were placed on the couch of Varian Clinac 21 EX linear accelerator, the spirit level was used for set up the position. The thickness of solid water phantom after the depth of measurement was 15 cm for complete scatter radiation.
- 2) The diamond detector was inserted in the phantom in the direction perpendicular to the central beam axis. The center of the diamond detector was at the depth of 1.5 cm and source-surface distance was set to 100 cm on the surface of solid water phantom.
- 3) 6MV photon beam of field size of  $10 \times 10 \text{ cm}^2$  was used.
- 4) The diamond detector cable was connected to the Dose 1 electrometer and operation bias of +100V was applied.

### 3.6.1.2. Polarization Effect

Since the response of the diamond detector depends on the creation and moving of electron-hole pair inside the diamond crystal, so the polarization effect affect the response of the diamond detector. Pre-irradiation dose can solve this effect as describe in section 2.1.4.4 Polarization effect Chapter II. Thus, polarization effect study was performed for investigating the pre-irradiation dose which is required for stabilize the response of the diamond detector.

#### *Procedure*

- 1) Used the typical measurement setup.
- 2) The diamond detector was irradiated by 6 MV photon beams. The radiation was delivered to 20 Gy in 0.5 Gy steps. Each success step of measurement, the electrometer readout (nC) were collected and continued without pause or stop the electrometer until the diamond detector was received 20Gy.
- 3) The response values of each 0.5 Gy step were normalized to the dose of 20 Gy.
- 4) The pre-irradiation dose was considered from the dose stabilized the detector response with standard deviation equal or less than 0.1%. [2]

### 3.6.1.3. Repeatability and Reproducibility

This study was performed to evaluate the diamond detector response versus times, or repeatability and reproducibility of diamond detector response. Repeatability study was performed within 10 min. immediately after pre-irradiation dose process was finish and reproducibility was observed from the results of repeatability study once a week over period of month.

#### *Procedure*

- 1) The typical setup and pre-irradiation with doses from polarization study with 6 MV photon beam, field size of  $10 \times 10 \text{ cm}^2$ , depth of 1.5cm, and SSD 100 cm were undertaken.
- 2) After pre-irradiation, the diamond detector was irradiated with dose of 0.5 Gy for 10 times. Each success measurement, the electrometer readouts (nC) were collected.
- 3) The standard deviation of detector response was calculated. The repeatability was evaluated by this standard deviation.
- 4) Reproducibility was evaluated by standard deviation of average detector response of each 10 repeated measurement data.



### 3.6.1.4. Linearity of Response

Linearity of response study was performed to evaluate the constancy of diamond detector response to the given doses from 1 – 400 cGy.

#### *Procedure*

- 1) The typical setup and pre-irradiation with doses from polarization study with 6 MV photon beam, field size of  $10 \times 10 \text{ cm}^2$ , depth of 1.5 cm, and SSD 100 cm were undertaken.
- 2) After pre-irradiation, the diamond detector was irradiated and 3 measurements were undertaken for each given dose from 1-400 cGy. Each success measurement, the electrometer readout (nC) was collected.
- 3) The given doses were 1, 2, 3, 4, 5, 10, 20, 30, 50, 100, 150, 200, 250, 300, and 400 cGy.
- 4) The electrometer readout of each given dose data set were averaged. The averaged readout were the response of detector (nC) which were calculated for detector sensitivity (nC/cGy)
- 5) Constancy of detector sensitivity to given dose of 1-400 cGy were evaluated for linearity of response of diamond detector. Moreover, linearity of response was also evaluated by R-square value of the trend line of linear regression of the detector response and given doses.

### 3.6.1.5. Dose Rate Dependence

Since the dose rates depend on SSD, [5] the dose rates in this study were changed by varying SSD in 10 cm steps. Figure 3.12 shows the varied dose rate as inverse square law function to SSD in range of 80-140 cm. This limited range was due to the limitation of vertical couch movement and the possible gap between the top of phantom and collimator. The nominal dose rate at SSD of 100 cm is set to 300 MU/min.

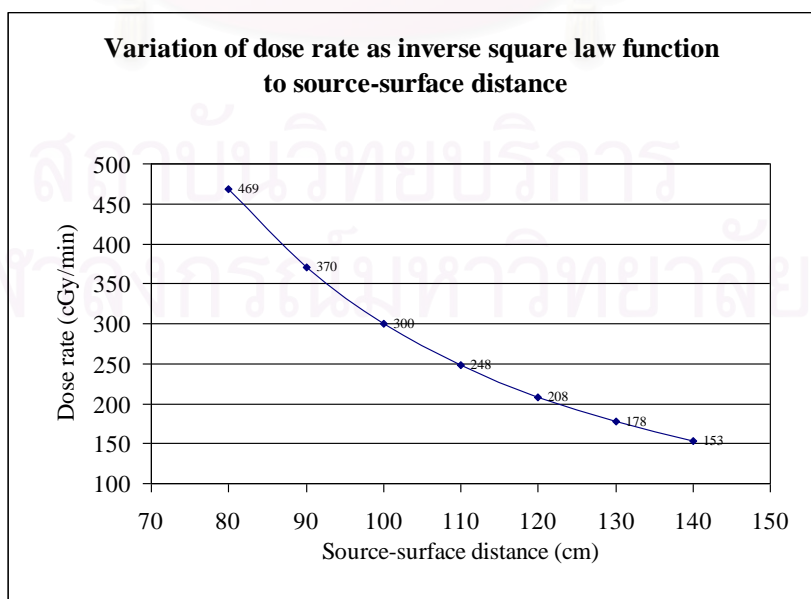


Figure 3.12 Variation of dose rate as inverse square law function to SSD.

### Procedure

- 1) The typical setup and pre-irradiation with doses from polarization study with 6 MV photon beam, field size of  $10 \times 10 \text{ cm}^2$ , depth of 1.5cm, and SSD 100 cm. were undertaken.
- 2) After pre-irradiation, the nominal dose rate was set to 300 MU/min at source-surface distance (SSD) of 100 cm and the diamond detector was irradiated with the dose of 0.5 Gy. The electrometer readout (nC) was collected.
- 3) Dose rate were varied by varying the SSD from 80-140 cm in 10 cm steps. The SSD were changed by moving the couch forward and backward to the gantry collimator. Figure 3.13 shows the set-up of the dose rate dependence study.
- 4) At each SSD, the diamond detector was irradiated with dose of 0.5 Gy at depth of 1.5cm in field size of  $10 \times 10 \text{ cm}^2$ , the electrometer readout (nC) .
- 5) An ionization chamber was irradiated under identical geometries and procedures. The electrometer readouts (nC) of ionization chamber were collected.
- 6) The ratio of diamond detector responses and ionization chamber responses were determined. These ratios were normalized at SSD of 100 cm.
- 7) Since the linac used in this study was set to 1MU for 1cGy in field size of  $10 \times 10 \text{ cm}^2$  at depth of maximum dose and SSD = 100 cm, The nominal dose rate of 300MU/min was assumed to 300cGy/min at same field size and SSD, so the dose rate in this study were varied between 153-469 cGy/min or 1.53-4.69 Gy/min..

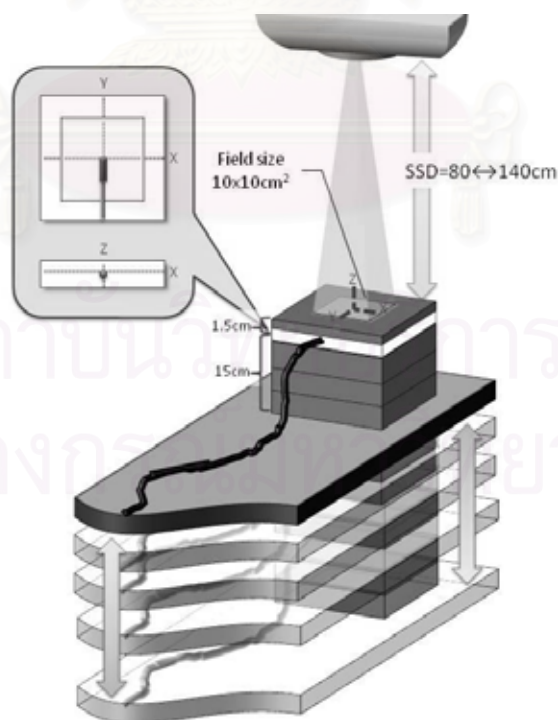


Figure 3.13 Set-up of the dose rate dependence study.

### 3.6.1.6. Beam Energy Dependence

To evaluate dependence of diamond detector response to beam energy, a study was performed for compared detector response in two beam energies of 6 MV and 10 MV. The ratio of the response of diamond detector to the response of an ionization chamber was determined.

#### *Procedure*

- 1) The typical setup and pre-irradiation with doses from polarization study with 6 MV photon beam, field size of  $10 \times 10 \text{ cm}^2$ , depth of 1.5cm, and SSD 100 cm. were undertaken.
- 2) The center of the diamond detector was set at the depth of 10 cm and irradiated with 6 MV photon beam in field size of  $10 \times 10 \text{ cm}^2$  with the dose of 1 Gy for 3 times. The electrometer readouts (nC) were averaged and collected.
- 3) At the same point, diamond detector was irradiated with 10 MV for 3 times of 1Gy. The electrometer readouts (nC) were collected.
- 4) An ionization chamber was irradiated under identical geometries for determined absorbed doses in both energies with procedures according to IAEA TRS 398. [16]
- 5) Responses of diamond detector were calculated for detector sensitivity with known dose obtained by ionization chamber.
- 6) The difference of the response for 6 MV and 10 MV was evaluated as dependence on beam energy.

### 3.6.1.7. Directional Dependence

In this study, the diamond detector was set up in two configurations; Figure 3.14 shows diagram of both configurations; perpendicular to central beam axis and parallel to central beam axis. The diamond detector response was measured in every  $30^\circ$  of direction of photon beam according to gantry rotation position.

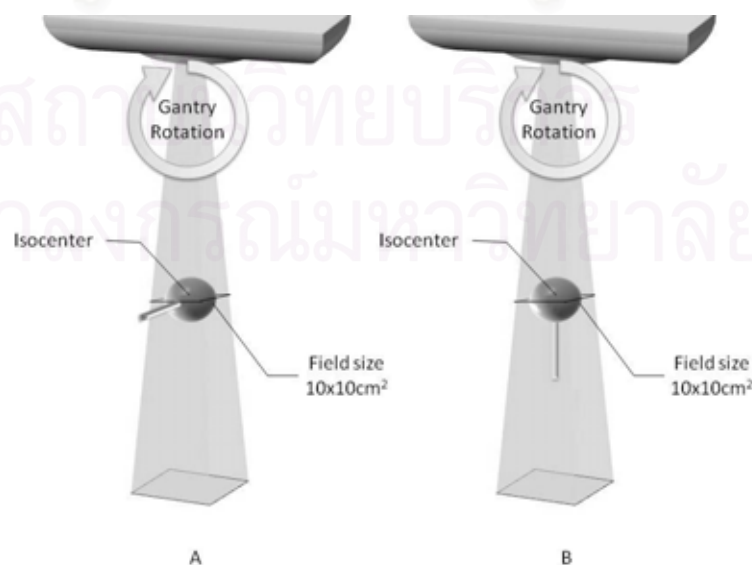


Figure 3.14 Diamond detector configurations in directional dependence study; (A) Perpendicular to central beam axis, (B) Parallel to central beam axis.

### *Procedure*

- 1) The diamond detector was placed in an in house build up cap made from paraffin wax which has diameter of 4.6 cm and placed them air by a custom plastic holder rod. The center of the diamond detector was at the isocenter of linac.
- 2) The diamond detector cable was connected to the Dose 1 electrometer and operation bias of +100V was applied.
- 3) 6 MV photon beams and field size of  $10 \times 10 \text{ cm}^2$  were used. Diamond detector was pre-irradiated if necessary.
- 4) After, the diamond detector was irradiated with dose of 0.5 Gy for 3 times in each directions of radiation beam. Each measurement, the electrometer readout (nC) was collected.
- 5) The electrometer readouts of each direction were averaged and evaluated as response of diamond detector in each beam direction. These response values were normalized to the  $0^\circ$  of beam direction in each data set of both configurations.

### **3.6.2. Performance of Diamond Detector**

After characterization of diamond detector, its dosimetric performances in small photon beam were evaluated by measurement of output factor, depth dose curves, and beam profiles. The measurement were performed in field size of  $10 \times 10 \text{ cm}^2$  and small field size of  $4 \times 4 \text{ cm}^2$ ,  $3 \times 3 \text{ cm}^2$ ,  $2 \times 2 \text{ cm}^2$ , and  $1.5 \times 1.5 \text{ cm}^2$ .

#### **3.6.2.1. Setup of Measurement**

Solid water phantom were used for output measurement performed with three detectors i.e. diamond detector, CC13, and silicon diode. And the blue phantom was used for depth dose curve and beam profile measurement performed with CC13 and silicon diode. The specific setup for each phantom and detector are described below.

For measurement in solid water phantom:

### *Procedure*

- 1) Solid water phantom were placed on the couch of Varian Clinac 21 EX linear accelerator, the spirit level was used for set up the position. The thickness of solid water phantom after the depth of measurement is 15 cm for complete scatter radiation.
- 2) The detector was placed in the phantom perpendicular to the central beam axis configuration.
  - a. For measurement performed by diamond detector. The canter of the detector was set at the depth of 1.5 cm in phantom and source-surface distance was set to 100 cm. The diamond detector cable was connected to the Dose 1 electrometer and operation bias of +100V was applied. The detector was pre-irradiated by an appropriate dose.
  - b. For measurement performed by silicon diode. The canter of the detector was set at the depth of 1.5 cm in phantom and source-

surface distance was set to 100 cm. The silicon diode cable was connected to the Dose 1 electrometer without operation bias applied. The detector was pre-irradiated by an appropriate dose.

- c. For measurement performed by CC13 ionization chamber. The center of the detector was set at the depth of 1.5 cm in phantom and source-surface distance was set to 100 cm. The chamber cable was connected to the Dose 1 electrometer and operation bias of +300V was applied.

For measurement in Blue phantom:

#### *Procedure*

- 1) Blue phantom was placed under the gantry of Varian Clinac 21 EX linear accelerator, the spirit level and the cross-hairs on the walls and bottom of the tank were used for set up the position. The source-surface distance was set to 100 cm.
- 2) The detector was placed on detector holder;
  - a. For measurement performed by CC13, the detector axis was perpendicular to the central beam axis configuration. Its effective point was displaced for 1.8 mm from detector center which is equal to  $0.6r$  where  $r$  is radius of detector sensitive volume. The CC13 was connected to the Dose 1 electrometer with +300V operation bias applied.
  - b. For measurement performed by silicon diode, the detector axis was parallel to the central beam axis configuration. Its effective point was displaced for 0.8 mm under the detector surface. The diode was connected to the Dose 1 electrometer without operation bias applied.
- 3) The position and limits of detector movement were set for center, water surface, and tank borders.
- 4) Beside the measured detector, another ionization chamber was used as reference detector. This detector was placed in plastic rod and placed in air under the collimator. Its sensitive volume was inside the beam but near the edge of beam.

#### **3.6.2.2. Output Measurement**

Output factor measurement is the determination of the dose rate at a reference depth for each small field size divided by the dose rate at the same point and depth for the reference field size of  $10 \times 10 \text{ cm}^2$ . In this study, diamond detector, silicon diode, and CC13 ionization chamber were employed for output measurements with the identical setting condition.

#### *Procedure*

- 1) The typical setup which specific to each detector was undertaken.
- 2) The 6 MV photon beam, depth of 1.5cm, and SSD 100 cm were set.
- 3) The radiation doses were measured by the detector 3 times for each field size. i.e. field size of  $1.5 \times 1.5$ ,  $2 \times 2$ ,  $3 \times 3$ ,  $4 \times 4$ , and  $10 \times 10 \text{ cm}^2$



- 4) The electrometer readouts of each field size were averaged. These averaged values were normalized to field size of  $10 \times 10 \text{ cm}^2$ . The normalized values were output factors of each field size.
- 5) Output factors obtained by each detector were compared to each other especially diamond detector.

### 3.6.2.3. Depth Dose Curve Measurement

Depth dose curve measurement is the determination of the absorbed dose at any depth to the absorbed dose at a fixed reference depth along the central beam axis of radiation beam. In this study, the fixed reference depth was the depth of maximum dose of 6 MV photon beam (1.5 cm). Diamond detector, silicon diode, and CC13 ionization chamber were employed for depth dose curve measurements with the same setting condition in reference field size of  $10 \times 10 \text{ cm}^2$  and small field sizes of  $4 \times 4$ ,  $3 \times 3$ ,  $2 \times 2$ , and  $1.5 \times 1.5 \text{ cm}^2$ .

#### *Procedure*

- 1) The typical setup which specific to each detector was undertaken.
- 2) The 6 MV photon beam, field size of  $10 \times 10 \text{ cm}^2$ , and SSD 100 cm were set.
- 3) The absorbed doses were measured by the detector in 0.2 cm step at the depth of 0.5 - 3 cm and 5 cm step at the depth deeper than 5 cm.
- 4) The obtained values of absorbed dose at any depth were normalized to the absorbed at the depth of 1.5 cm as percentage relation.
- 5) Depth dose curve obtained by each detector were compared to each other especially diamond detector. The criteria of consideration are in the section 3.4 Data analysis in this chapter.

### 3.6.2.4. Beam Profile Measurement

Beam profile measurement is the determination of the dose variation across the radiation field at a specified depth. In this study, the specified depth was the depth of maximum dose of 6 MV photon beam (1.5 cm). Diamond detector, silicon diode, and CC13 ionization chamber were employed for beam profile measurements with the same setting condition. The beam profiles were extensively measured over the edge of each field size in both sides along the transverse axis

#### *Procedure*

- 1) The typical setup which specific to each detector was undertaken.
- 2) 6 MV photon beam, depth of 1.5 cm, and SSD 100 cm were set.
- 3) Field size of  $10 \times 10 \text{ cm}^2$  and small field sizes of  $4 \times 4$ ,  $3 \times 3$ ,  $2 \times 2$ , and  $1.5 \times 1.5 \text{ cm}^2$  were used.
- 4) The doses were measured in 1 mm step in the range of  $\pm 0.5 \text{ cm}$ . at the edge of the radiation field and 1 cm step at the rest of the field.
- 5) Beam profiles obtained by each detector were compared to each other especially diamond detector. The criteria of consideration are in the section 3.4 Data analysis in this chapter.

### 3.7. Data Collection

The measurements were performed in the Varian 21EX room at Division of Radiation Oncology, Department of Radiology, King Chulalongkorn Memorial Hospital. All measurements were supervised by medical physicist from Chulalongkorn University and King Chulalongkorn Memorial Hospital.

### 3.8. Data Analysis

#### 3.8.1. Characteristics of Diamond Detector

In characteristics studies, the data were analyzed and interpreted with specified criteria of each work. Table 3.2 shows criteria of each characteristics study.

Table 3.2 Criteria in characteristics study. [2]

Characteristics studies	Criteria
Polarization effect	The accumulated dose that stabilized detector response with SD less than 0.1% after normalized at the highest dose was pre-irradiation dose.
Repeatability and reproducibility	Repeatability was evaluated by standard deviation of 10 repeated measurements. Reproducibility was evaluated by standard deviation of averaged detector sensitivity from each repeated measurements. These standard deviations should be less than 1%.
Linearity of response	Linearity of response was evaluated by the same detector sensitivity to any given dose and R-square value of trend line in linear regression function should be equal to 1.
Dose rate dependence	Independence on dose rate was evaluated by the diamond detector to reference chamber response ratio on difference dose rate was equal to 1
Beam energy dependent	Independence on beam energy was evaluated by the diamond detector to reference chamber response ratio in 6 MV photon beam was similar to those ratio in 10 MV photon beam
Directional dependence	Independence on direction was evaluated by normalized detector response equal to 1

#### 3.8.2. Performance of Diamond Detector

For the performance in small photon beam of diamond detector, its obtained beam data were compared with those obtained by CC13 and silicon diode. The set of beam data in the study consist of output factor, depth dose curve, and beam profile. For output factor, the criteria was in agreement on output factor values after normalized at field size of  $10 \times 10 \text{ cm}^2$ , the deviation should be in 1%. [2] For depth dose curve and beam profile, the concept of the criteria for acceptability of dose calculations recommended by Van Dyk *et al* [17-18] and Venselae *et al* [19] were used.

Criteria for acceptability of dose calculations by *Venselaar et al* expressed some criteria for compared calculated and measured dose value in beam data used in treatment planning system. This paper was applied this criteria for comparing the measured dose values from difference detectors. The deviations between data of diamond detector ( $D_{\text{diamond}}$ ) and the others ( $D_{\text{detector}}$ ) can be expressed as a percentage by  $\delta$  value from the following equation:

$$\delta = 100\% \times (D_{\text{diamond}} - D_{\text{detector}}) / D_{\text{detector}}$$

Difference  $\delta$  is proposed for different regions in the beam. Figure 3.15 shows the regions of validity of the criteria.

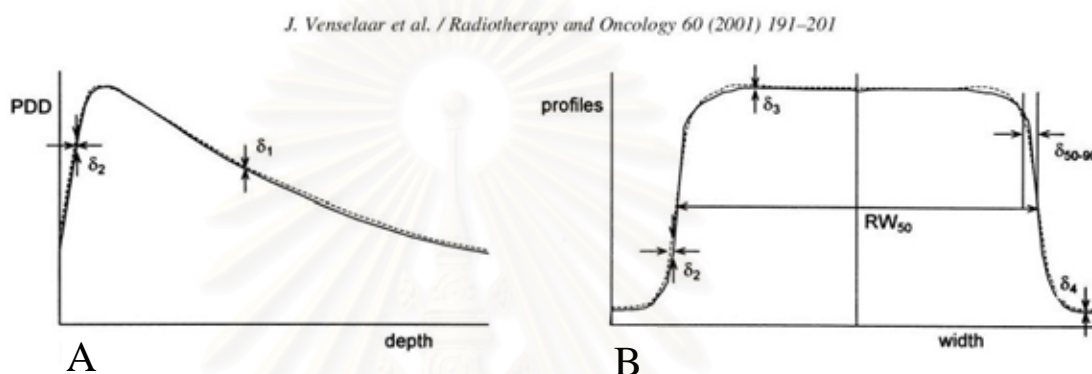


Figure 3.15 Regions of validity of the criteria  $\delta_1$ - $\delta_4$ , radiological width  $RW_{50}$ , and beam fringe  $\delta_{50-90}$  in (A) depth dose curve and (B) beam profile

In this paper, the criteria  $\delta_1$ - $\delta_3$ ,  $RW_{50}$ , and  $\delta_{50-90}$  were used, definition of criteria as:

- $\delta_1$ : for data points on the central beam axis beyond the depth of  $d_{\text{max}}$ : the high dose and small dose gradient region.
- $\delta_2$ : for data points in the build-up region, in the penumbra, and in regions close to interfaces of inhomogeneities: the high dose and large dose gradient regions. This criterion can be applied in the region between the phantom surface and the depth of the 90% isodose surface, as well as in the penumbra region.
- $\delta_3$ : for data points beyond  $d_{\text{max}}$ , within the beam but outside the central beam axis: again this region is a high dose and small dose gradient region.
- $RW_{50}$ : the radiological width, defined as the width of a profile measured at half its height compared to the value at the beam axis.
- $\delta_{50-90}$ : the distance between the 50% and the 90% point (relative to the maximum of the profile) in the penumbra, which is sometimes called 'beam fringe'

Table 3.3 shows summary of regions of validity of the  $\delta_1$ - $\delta_4$ , radiological width  $RW_{50}$ , and beam fringe  $\delta_{50-90}$ . The criteria  $\delta_1$  and  $\delta_2$  were used for comparison of depth dose curve and criteria  $\delta_1$ - $\delta_4$ ,  $RW_{50}$ , and  $\delta_{50-90}$  were used for comparison of beam profiles which also used determination of penumbra of dose of 80%-20%.

**Table 3.3** Summary of regions of validity of the  $\delta_1$ - $\delta_4$ , radiological width  $RW_{50}$ , and beam fringe  $\delta_{50-90}$  criteria.

Criteria	Regions of validity
$\delta_1$	(central beam axis data) high dose, small dose gradient
$\delta_2$	(build-up region of central beam axis, penumbra region of the profile) high dose, large dose gradient
$\delta_3$	(outside the central beam axis region) high dose, small dose gradient
$RW_{50}$	(radiological width)
$\delta_{50-90}$	(beam fringe)

### 3.8.3. Uncertainty Evaluation [3]

The uncertainty in the output factor measurements was evaluated, according to the IAEA TRS-398 [16] dosimetry protocol combining two different contributions: establishment of the measurement conditions (0.4%, 1 standard deviation, SD) and dosimeter reading relative to beam monitor (0.6%, 1 SD). These values are quoted in the same IAEA protocol [16] as well. Hence, a global uncertainty in the OF ratio of 1% (1 SD) is estimated. This evaluation does not take into account possible effects coming from the unsuitable spatial resolution of the detector and from the difficulty of a correct detector positioning in narrow fields.

The uncertainty in PDD measurements can be separately considered for the ascending and descending parts of the curve. In the first case, because of the high dose gradient, it is not proper to assess the uncertainty on the dose, but it is more meaningful to evaluate the positional uncertainty, which is mainly due to the difficulty on setting the zero position of the detector at the water surface and which can be estimated to about 0.5 mm. Thus, for comparison of PDDs obtained with different detectors, a  $\delta_2$  less than 1 mm was considered not significant. For the region after the depth of maximum dose, due to the lower gradient, a shift of 0.5 mm in depth determines an error in dose of less than 0.2% (in correspondence of the maximum gradient position). In this case, the contributions to the uncertainty in dose assessment come from establishment of setup (0.4%), stability of the field detector/electrometer assembly (0.3%) and reference detector/electrometer assembly (0.3%). This leads to a combined uncertainty of about 0.6% (1 SD). Therefore, for comparison of PDDs obtained with different detectors, percentage dose differences less than 1% were considered not significant. Again, this evaluation does not take into account effects coming from unsuitable spatial resolution of the detector.

When transverse profiles are analyzed, the uncertainties are significantly different if ion chamber or solid-state dosimeters are employed. In the first case the averaging effect in the sensitive volume cannot be neglected even if measurements are performed in regions where the dose profile has an almost linear shape. Thus, 1 mm, equal to half cavity radius, is assumed as an upper limit for the uncertainty in penumbra and field width evaluation. On the contrary, with silicon diode, due to its small thickness, the measurement uncertainty can be attributed mainly to the positional reproducibility of the water phantom (0.1 mm) so that both the parameters are measured with an uncertainty of 0.2 mm. Diamond lies between the two previous cases: considering an averaging effect of 0.15 mm (half thickness), in addition to the

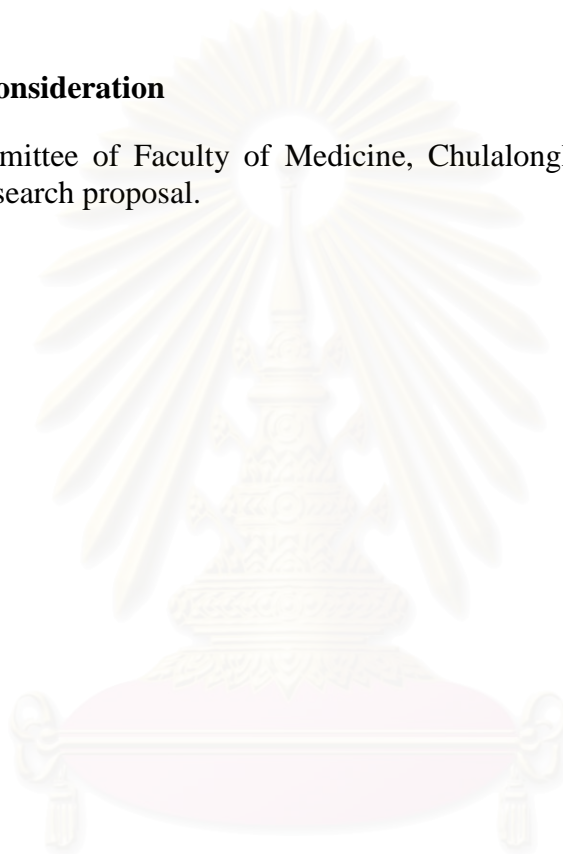
reproducibility error of 0.2 mm, leads to a combined uncertainty of about 0.3 mm in the penumbra and field width evaluation.

### **3.9. Expected Benefit and Application**

This study is designed to study the characteristics and dosimetric performance in small photon beam of diamond detector. The aim of the study was to understand the characteristics of the detector and use it in dosimetric applications especially in small field photon dosimetry.

### **3.10. Ethic Consideration**

Ethics Committee of Faculty of Medicine, Chulalongkorn University has been approved the research proposal.



สถาบันวิทยบริการ  
จุฬาลงกรณ์มหาวิทยาลัย



## CHAPTER IV

### RESULTS

The diamond detector was investigated for its characteristic and then evaluated its dosimetric performance in small photon beams by comparison with CC13 ionization chamber and silicon diode detector.

#### 4.1. Characteristics of Diamond Detector

##### 4.1.1. Polarization Effect

Figure 4.1 and Table 4.1 show the variations of diamond detector sensitivity with the accumulated dose. Detector sensitivity values were normalized to the dose of 20 Gy. The detector response reached stability after an accumulated dose of 5 Gy with a total decrease of 2%. The standard deviations (SD) of detector sensitivity in stable region were less than 0.1%.

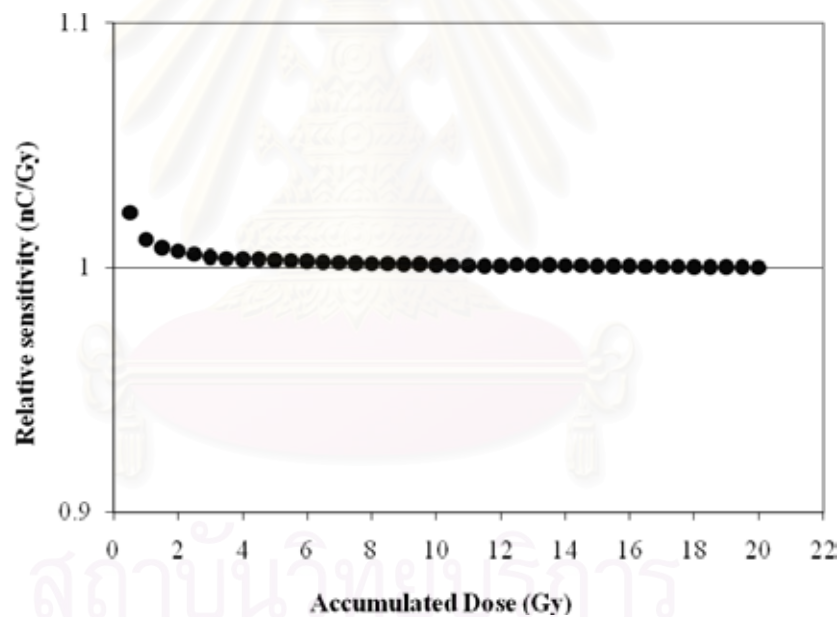


Figure 4.1 Variations of diamond detector sensitivity with the accumulated dose at depth of 1.5 cm for 6 MV photon beams, given in 0.5 Gy steps, SSD = 100 cm.

**Table 4.1** Variations of diamond detector sensitivity with the accumulated dose at depth of 1.5 cm for 6 MV photon beams, given in 0.5 Gy steps, SSD = 100 cm.

Accumulated dose (Gy)	Response (nC)	Sensitivity (nC/Gy)
0.5	53.3	1.065
1	105.4	1.054
1.5	157.6	1.051
2	209.8	1.049
2.5	261.9	1.048
3	314.0	1.047
3.5	366.1	1.046
4	418.3	1.046
4.5	470.6	1.046
5	522.6	1.045
5.5	574.8	1.045
6	626.9	1.045
6.5	678.8	1.044
7	730.9	1.044
7.5	783.0	1.044
8	835.0	1.044
8.5	887.1	1.044
9	939.2	1.044
9.5	991.3	1.043
10	1043.0	1.043

สถาบันวิทยบริการ  
จุฬาลงกรณ์มหาวิทยาลัย

Table 4.1(cont.) Variations of diamond detector sensitivity with the accumulated dose at depth of 1.5 cm for 6 MV photon beams, given in 0.5 Gy steps, SSD = 100 cm.

Accumulated dose (Gy)	Response (nC)	Sensitivity (nC/Gy)
10.5	1095	1.043
11	1147	1.043
11.5	1199	1.043
12	1251	1.043
12.5	1304	1.043
13	1356	1.043
13.5	1408	1.043
14	1460	1.043
14.5	1512	1.043
15	1564	1.043
15.5	1616	1.043
16	1668	1.043
16.5	1720	1.042
17	1772	1.042
17.5	1824	1.042
18	1876	1.042
18.5	1928	1.042
19	1980	1.042
19.5	2032	1.042
20	2084	1.042

สถาบันวิทยบริการ  
จุฬาลงกรณ์มหาวิทยาลัย

#### 4.1.2. Repeatability and Reproducibility

For repeatability, with pre-irradiation dose of 5 Gy, the standard deviation of diamond detector sensitivity in each 10 repeated readings for four times of measurement were within 0.16%. Table 4.2 shows detector sensitivity values and standard deviations of each data set. For reproducibility which was evaluated by means of the average value of each repeated data set, the standard deviation of 4 week measurements was 0.4%. Variations of detector sensitivity for all 10 repeated and 4 times of measurements were in the range of 1.042-1.055 nC/cGy.

**Table 4.2** Variations of diamond detector sensitivity of 10 repeated measurements after pre-irradiation. Performed once a week for 6 MV photon beams,  $10 \times 10$  cm<sup>2</sup> field size at depth of 1.5 cm, SSD = 100 cm.

Number of measurement	Detector sensitivity (nC/cGy)			
	1 <sup>st</sup> week	2 <sup>nd</sup> week	3 <sup>rd</sup> week	4 <sup>th</sup> week
1	1.047	1.047	1.045	1.051
2	1.047	1.047	1.045	1.050
3	1.045	1.045	1.042	1.055
4	1.047	1.047	1.042	1.052
5	1.046	1.046	1.045	1.055
6	1.044	1.044	1.043	1.052
7	1.046	1.046	1.043	1.051
8	1.047	1.047	1.044	1.052
9	1.045	1.045	1.042	1.051
10	1.045	1.045	1.043	1.051
Mean	1.046	1.046	1.043	1.052
SD	0.10%	0.10%	0.13%	0.16%

### 4.1.3. Linearity of Response

Figure 4.2 and Table 4.3 show the variations of diamond detector response and sensitivity to the given doses in the range of 1-400 cGy. The detector sensitivity was stable and showed linearity of response to the given dose. Linearity of response was also evaluated by R-square value = 1 of the trend line of linear regression between the detector response and given doses.

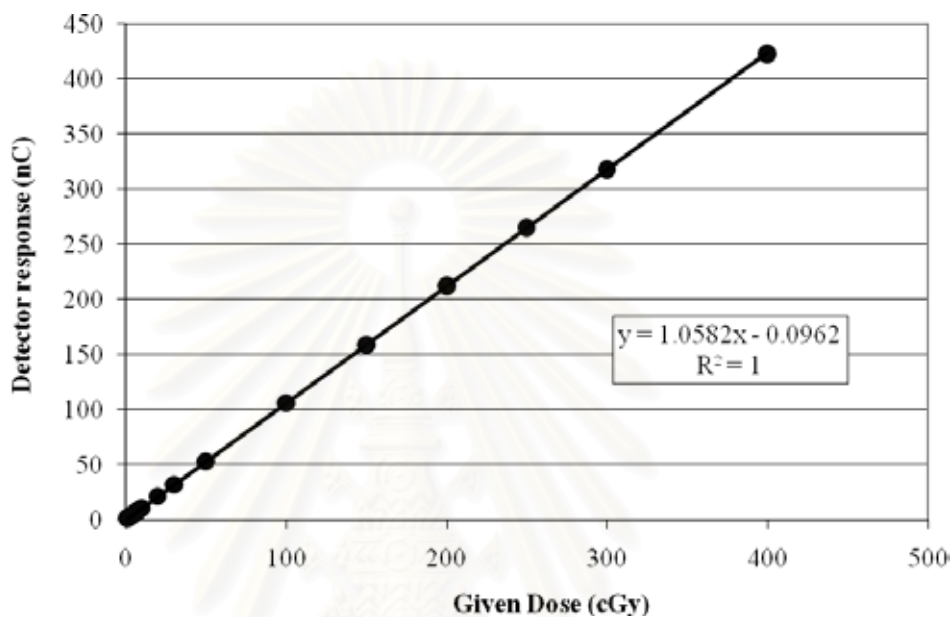


Figure 4.2 Variations of diamond detector response to the given doses of 1-400 cGy at depth of 1.5 cm for 6 MV photon beam, SSD = 100 cm.



**Table 4.3** Variations of diamond detector response to given dose of 1-400 cGy for 6 MV photon beams, 10×10 cm<sup>2</sup> field size, 1.5 cm depth, SSD = 100 cm.

Given dose (cGy)	Detector response (nC)	Sensitivity (nC/cGy)
1	1.06	1.06
2	2.10	1.05
3	3.13	1.04
4	4.14	1.04
5	5.20	1.04
6	6.28	1.05
7	7.30	1.04
8	8.35	1.04
9	9.40	1.04
10	10.48	1.05
20	20.98	1.05
30	31.55	1.05
50	52.66	1.05
100	105.60	1.06
150	158.53	1.06
200	211.70	1.06
250	264.77	1.06
300	317.65	1.06
400	422.80	1.06

สถาบันวิทยบริการ  
จุฬาลงกรณ์มหาวิทยาลัย

#### 4.1.4. Dose Rate Dependence

Figure 4.3 and Table 4.4 show the variations of the ratio between diamond detector response to reference chamber response and the dose rate ranged from 1.53 to 4.69 Gy/min. The detector responses were normalized to the dose rate of 3 Gy/min. The diamond to ion chamber response ratios were 1.008 to 0.995 for dose-rate varied from 1.58 to 4.69 Gy/min. So, the diamond detector showed slightly dose rate dependence, the response has decreased when dose rate has increased.

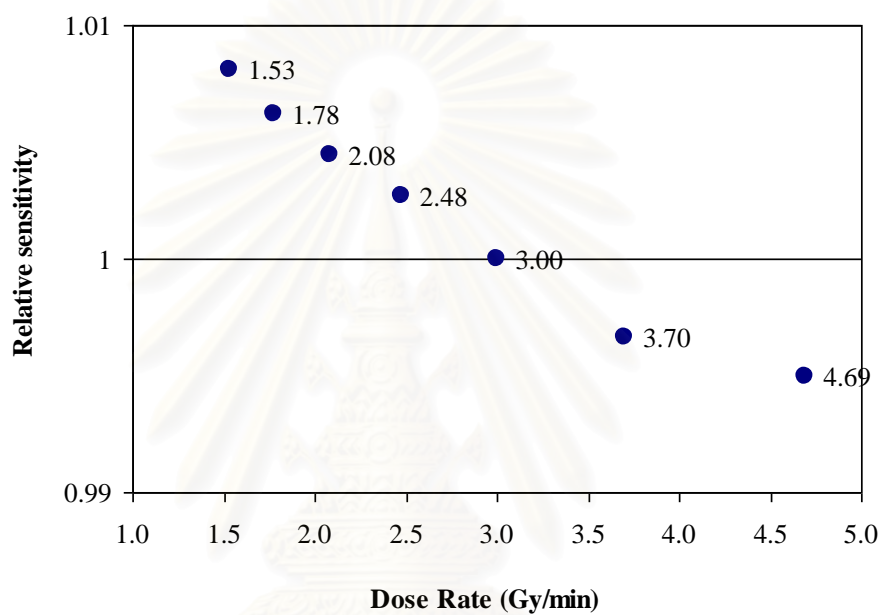


Figure 4.3 Variations of diamond detector sensitivity versus dose rate varied from 1.53–4.63 Gy/min for 6 MV photon beams,  $10 \times 10$  cm<sup>2</sup> field size at depth of 1.5 cm.

**Table 4.4** Variations of diamond detector sensitivity versus dose rate, for 6 MV photon beams, 10×10 cm<sup>2</sup> field size at depth of 1.5 cm.

Dose rate	Diamond detector response (nC)	Reference chamber response (nC)	Diamond to reference chamber response ratio	Relative sensitivity
1.53	48.280	1.696	28.46	1.008
1.78	55.667	1.960	28.41	1.006
2.08	64.670	2.285	28.30	1.002
2.48	76.053	2.687	28.31	1.003
3.00	90.643	3.211	28.23	1.000
3.70	109.800	3.902	28.14	0.997
4.69	136.500	4.859	28.09	0.995

#### 4.1.5. Beam Energy Dependence

Table 4.5 shows diamond detector response compared with absorbed dose measured by reference chamber in 6 and 10 MV photon beam. The result showed energy independence of diamond detector. The difference of the response for 6 MV and 10 MV was 0.04%.

**Table 4.5** Response of diamond detector and reference chamber for 6 and 10 MV photon beam, field size of 10×10 cm<sup>2</sup> at depth of 10 cm, SSD = 100 cm, and given dose of 100 MU.

Beam energy	Diamond detector response (nC)	Reference Chamber absorbed dose (cGy)	Diamond detector sensitivity (nC/cGy)
6 MV	70.1	66.37	1.056
10 MV	76.3	72.20	1.057
		Difference	0.04%

#### 4.1.6. Directional Dependence

Figure 4.4 and Table 4.6 show variations of diamond detector response to every  $30^\circ$  of beam directions in both configurations; Perpendicular and parallel to central beam axis. The response values were normalized to beam direction of  $0^\circ$ . The maximum deviations were 1% and 1.4% in perpendicular and parallel configuration, respectively.

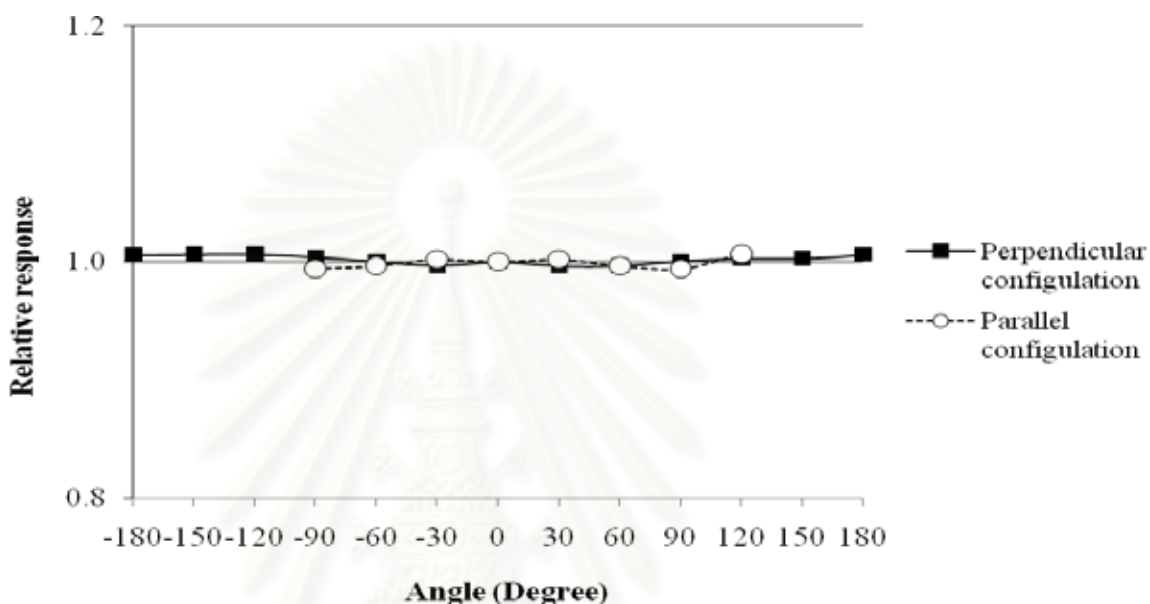


Figure 4.4 Variations of diamond detector response to the beam directions for 6 MV photon beams, measured free in air at isocenter.

**Table 4.6** Variations of diamond detector response to the beam directions, in 6 MV photon beams, 10×10 cm<sup>2</sup> field size, source to the center of detector = 100 cm. (N/P = Not Perform).

Beam direction	Relative detector response	
	Perpendicular configuration	Parallel configuration
0	1.0000	1.0000
30	0.9966	1.0019
60	0.9967	0.9965
90	1.0009	0.9940
120	1.0030	1.0067
150	1.0029	N/P
180	1.0061	N/P
210	1.0066	N/P
240	1.0068	N/P
270	1.0042	0.9940
300	1.0004	0.9965
330	0.9967	1.0019



## 4.2. Performance of Diamond Detector

### 4.2.1. Output Factor Measurement

Figure 4.5 and Table 4.7 show output factor of 6 MV photon beam obtained by diamond detector, CC13 ionization chamber, and silicon diode detector. The values were normalized to field size of  $10 \times 10 \text{ cm}^2$  of each data set.

For field size of  $4 \times 4 \text{ cm}^2$  and  $3 \times 3 \text{ cm}^2$ , the output factors obtained by diamond detector and CC13 were comparable with differences of 0.1% and 0.2% for field size of  $4 \times 4 \text{ cm}^2$  and  $3 \times 3 \text{ cm}^2$ , respectively. The output factors of diamond detector were 0.8% and 0.9% higher than those from silicon diode for field size of  $4 \times 4 \text{ cm}^2$  and  $3 \times 3 \text{ cm}^2$ , respectively.

For field size of  $2 \times 2 \text{ cm}^2$ , output factors from diamond detector was 1% higher than both output factors obtained by CC13 and silicon diode while output factors of CC13 and silicon diode were comparable with 0.1% difference.

For field size of  $1.5 \times 1.5 \text{ cm}^2$ , the output factor obtained by diamond detector was 0.7% higher than those obtained by silicon diode. Output factor obtained by CC13 was 2.3% and 1.6% lower than diamond detector and silicon diode, respectively.

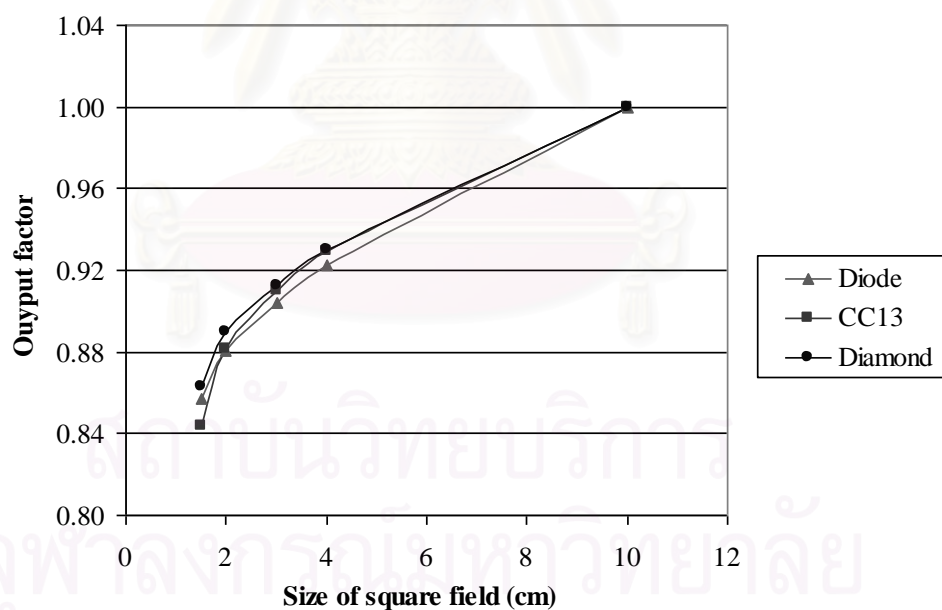


Figure 4.5 Output factors of 6 MV photon beam obtained by diamond detector, CC13 ionization chamber, and silicon diode detector, for field size of  $10 \times 10 \text{ cm}^2$  at depth of 1.5 cm, SSD = 100 cm.

**Table 4.7** Output factors of 6 MV photon beam obtained by Diamond detector, CC13 ionization chamber, and silicon diode detector, for field size of  $10 \times 10 \text{ cm}^2$  at depth of 1.5 cm, SSD = 100 cm.

Field size ( $\text{cm}^2$ )	Output factor		
	Diamond	CC13	Diode
$10 \times 10$	1.000	1.000	1.000
$4 \times 4$	0.930	0.929	0.923
$3 \times 3$	0.912	0.910	0.904
$2 \times 2$	0.890	0.882	0.880
$1.5 \times 1.5$	0.863	0.843	0.857

#### 4.2.2. Depth Dose Curve Measurement

Figure 4.6 - 4.10 show depth dose curves of 6 MV photon beams obtained by diamond detector, CC13 ionization chamber, and silicon diode detector for field sizes of  $10 \times 10$ ,  $4 \times 4$ ,  $3 \times 3$ ,  $2 \times 2$  and  $1.5 \times 1.5 \text{ cm}^2$ , respectively. The data of depth dose curves were considered according to the criteria in section 3.4 Data Analysis in Chapter III. Table 4.8-4.9 shows the differences between the depth dose curves obtained by diamond detector and the others. The criteria of  $\delta_1$  and  $\delta_2$  were used as the percent dose differences for the descending region and distance difference at the build up region of depth dose curve, respectively. Therefore for convenient, “diamond-CC13” was used throughout this section to represent the comparison between data obtained by diamond detector and CC13 while “diamond-diode” was used to represent the comparison between data obtained by diamond detector and silicon diode

For field size of  $10 \times 10 \text{ cm}^2$ , in build up region of depth dose curve, the depth dose curve obtained by diamond detector was comparable with CC13 and silicon diode. The  $\delta_2$  of diamond-CC13 were within 1.5 mm while  $\delta_2$  of diamond-diode were within 1.8 mm. In the descending region of the depth dose curves measured by three detectors were comparable and  $\delta_1$  were within 1% until the depth of 15 cm. At the depth deeper than 15 cm, the depth dose curve measured by diamond detector was lower than those measured by both CC13 and silicon diode. The  $\delta_1$  of diamond-CC13 were within 2.5% but  $\delta_1$  of diamond-diode were increased to 4% at depth of 28 cm.

For field size equal and smaller than  $4 \times 4 \text{ cm}^2$ , in build up region of depth dose curve, the depth dose curves obtained by diamond detector was higher than those obtained by the others except for field size of  $1.5 \times 1.5 \text{ cm}^2$ . For field size of  $4 \times 4 \text{ cm}^2$  to  $2 \times 2 \text{ cm}^2$ , the  $\delta_2$  of diamond to others were within 2.6 mm. For field size of  $1.5 \times 1.5 \text{ cm}^2$ ,  $\delta_2$  of diamond-CC13 and diamond-diode were 2.46 mm and 2.07 mm, respectively. In the descending region of all field size smaller than  $4 \times 4 \text{ cm}^2$ , depth dose curve obtained by diamond detector was slightly lower than CC13 at depth of 15 cm and lower than diode at the depth of 10 cm. For the deeper depth,  $\delta_1$  of diamond-CC13 and diamond-diode were increased to 4.7% and 4.6%, respectively.

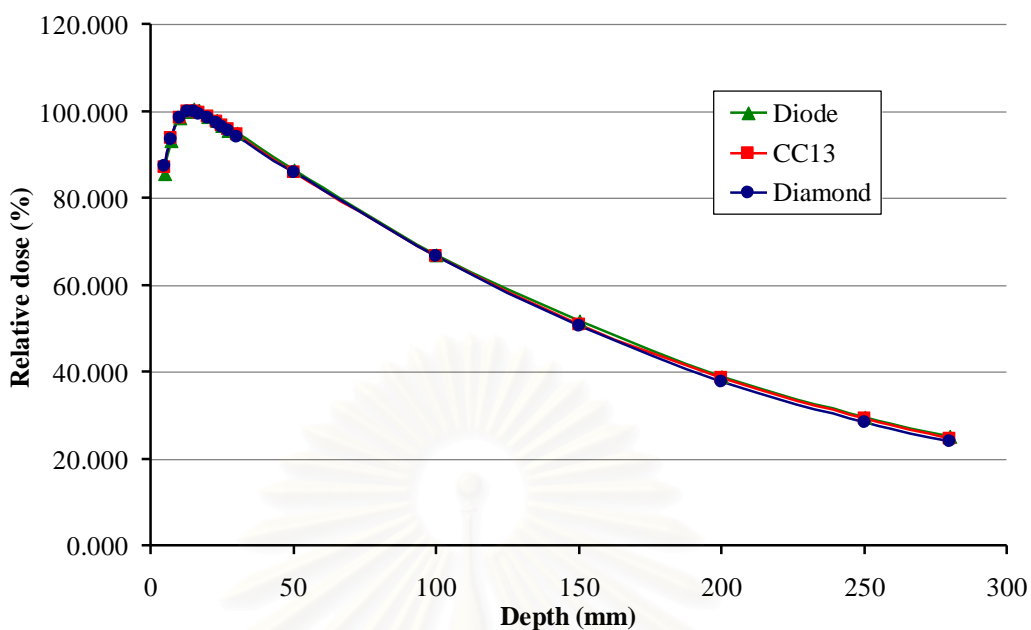


Figure 4.6 Depth dose curves of  $10 \times 10 \text{ cm}^2$  field size for 6 MV photon beams obtained by diamond detector, CC13 ionization chamber, and silicon diode detector.

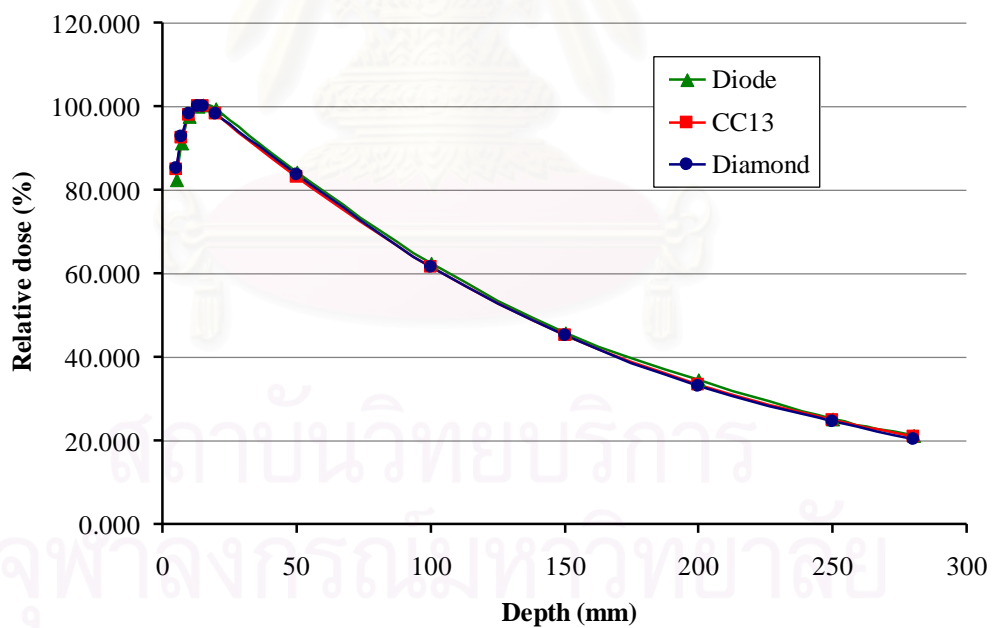


Figure 4.7 Depth dose curves of  $4 \times 4 \text{ cm}^2$  field size for 6 MV photon beams obtained by diamond detector, CC13 ionization chamber, and silicon diode detector.

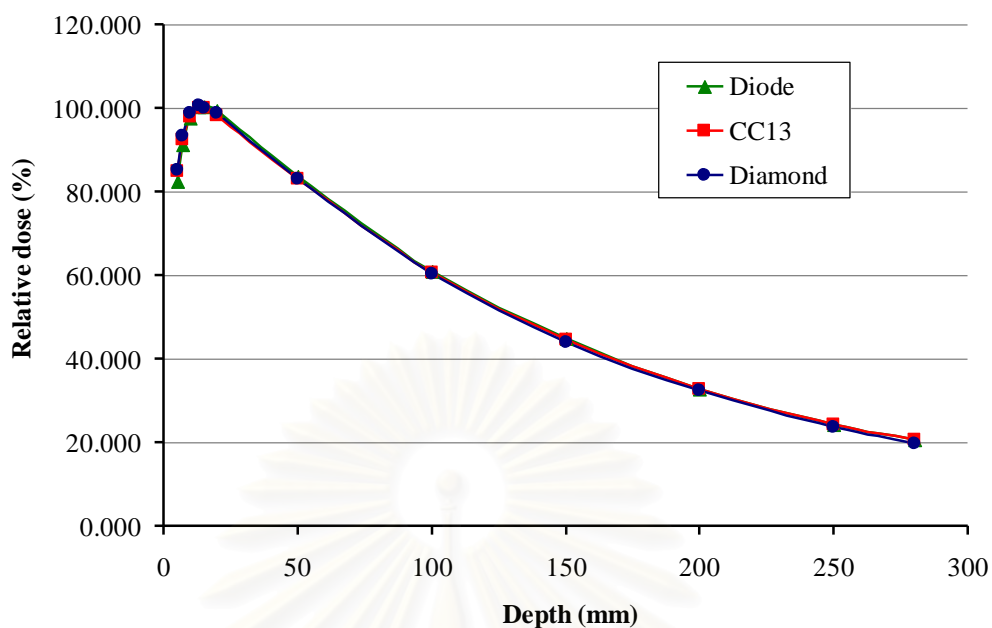


Figure 4.8 Depth dose curves of  $3 \times 3 \text{ cm}^2$  field size for 6 MV photon beams obtained by diamond detector, CC13 ionization chamber, and silicon diode detector.

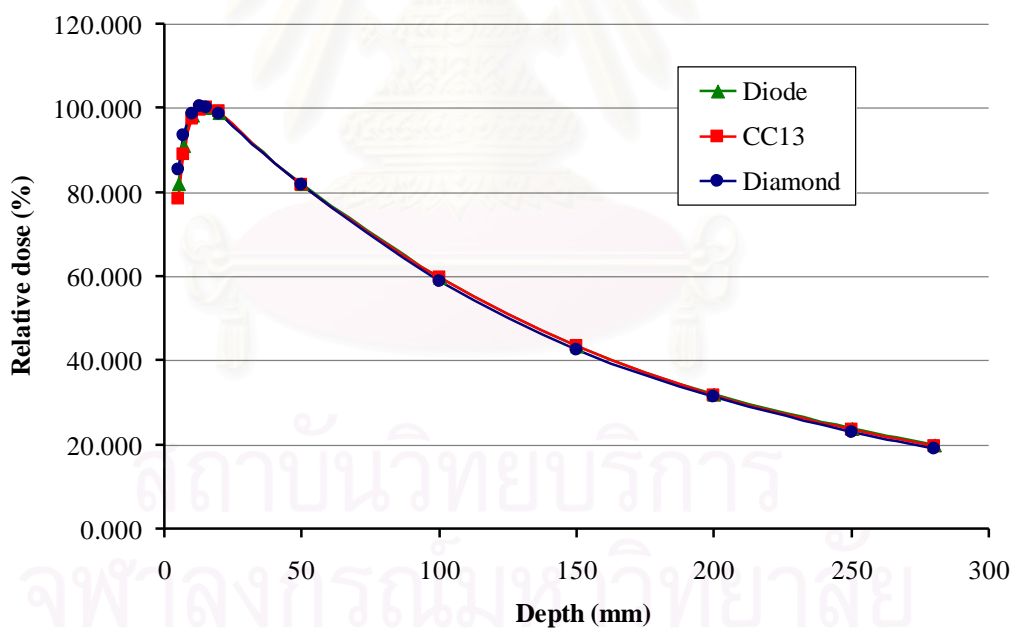


Figure 4.9 Depth dose curves of  $2 \times 2 \text{ cm}^2$  field size for 6 MV photon beams obtained by diamond detector, CC13 ionization chamber, and silicon diode detector.

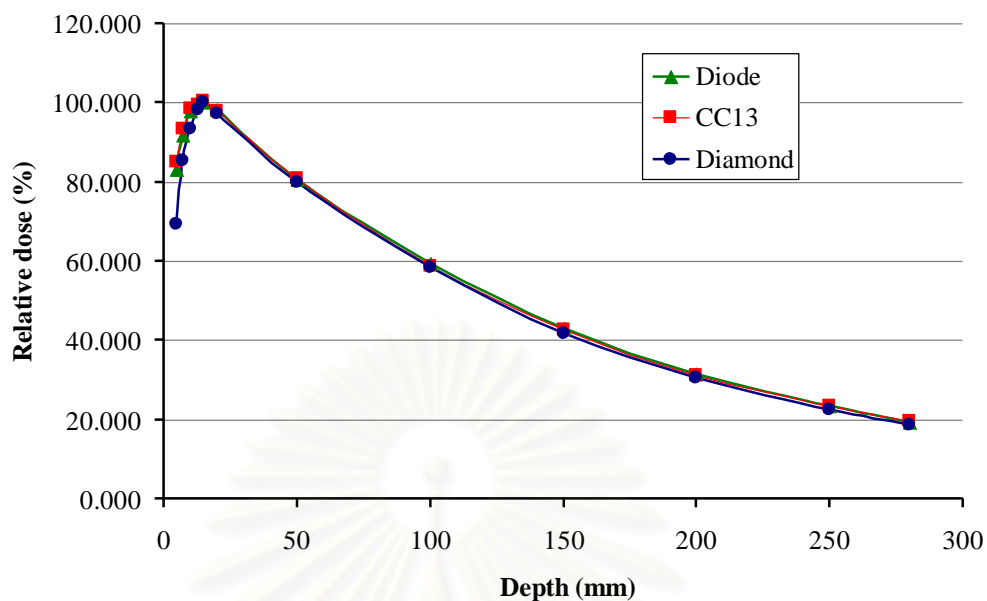


Figure 4.10 Depth dose curves of  $1.5 \times 1.5 \text{ cm}^2$  field size for 6 MV photon beams obtained by diamond detector, CC13 ionization chamber, and silicon diode detector.

**Table 4.8** The differences of build up region of depth dose curves of 6 MV photon beams obtained by diamond detector compared with those obtained by CC13 and silicon diode detector. The sign (+) indicates to deeper and the sign (-) indicates to more surface than data of diamond detector.

Dose (%)	Field size	$10 \times 10 \text{ cm}^2$		$4 \times 4 \text{ cm}^2$		$3 \times 3 \text{ cm}^2$		$2 \times 2 \text{ cm}^2$		$1.5 \times 1.5 \text{ cm}^2$	
		Criteria	CC13	Diode	CC13	Diode	CC13	Diode	CC13	Diode	CC13
70	$\delta 2$ (mm)	-	-	+2.03	+2.60	+1.77	+2.43	+2.62	+2.61	-2.00	-1.29
80		-	-	+0.71	+1.09	+0.62	+1.02	+1.60	+1.09	-1.95	-1.60
90		+1.51	+1.81	+0.77	+1.17	+1.06	+1.50	+2.27	+1.72	-2.46	-2.07



**Table 4.9** The differences of descending region of depth dose curves of 6 MV photon beams obtained by diamond detector compared with those obtained by CC13 and silicon diode detector. The sign (+) indicates to higher and the sign (-) indicates to lower than data of diamond detector.

Depth (cm)	Field size	10×10 cm <sup>2</sup>		4×4 cm <sup>2</sup>		3×3 cm <sup>2</sup>		2×2 cm <sup>2</sup>		1.5×1.5 cm <sup>2</sup>	
		Criteria	CC13	Diode	CC13	Diode	CC13	Diode	CC13	Diode	CC13
2		+0.33	+0.27	+0.08	+1.07	-0.45	+0.69	+0.39	+0.25	+0.56	+0.79
5		+0.15	+0.68	-0.67	+0.74	+0.06	+0.61	+0.04	+0.28	+1.13	+0.69
10		-0.22	+0.43	+0.23	+1.49	+0.67	+1.23	+1.25	+1.30	+0.67	+1.79
15	δ1 (%)	+0.67	+2.32	+0.37	+1.54	+1.30	+1.49	+1.59	+1.60	+2.83	+3.13
20		+1.93	+3.05	+0.61	+3.89	+1.41	+1.32	+1.16	+2.44	+1.87	+2.61
25		+2.50	+3.48	+2.00	+2.84	+2.70	+2.62	+2.21	+3.11	+3.23	+3.20
28		+2.17	+4.13	+2.47	+4.59	+3.74	+3.58	+3.71	+4.29	+4.75	+3.32

### 4.2.3. Beam Profile Measurement

Table 4.10 shows  $RW_{50}$ , beam fringe in the region of 50-90% and penumbra in the region of 20-80% dose. Table 4.11 shows the difference of beam profiles obtained by diamond detector to the others with the use of  $\delta_2$  for comparison at the edge of the beam and  $\delta_3$  for the region inside the beam. Figure 4.11 - 4.15 show beam profiles of 6 MV photon beams obtained by diamond detector, CC13 ionization chamber, and silicon diode detector for field sizes of 10×10, 4×4, 3×3, 2×2 and 1.5×1.5 cm<sup>2</sup>, respectively.

For field size of 10×10 cm<sup>2</sup>,  $RW_{50}$  of beam profile obtained by diamond detector was slightly larger than the others while the penumbra and beam fringe were slightly smaller than those by CC13 but slightly larger than those by silicon diode. The differences of  $RW_{50}$  by three detectors were within 1 mm. The difference of beam fringes and penumbra of diamond-CC13 were 0.12 and 0.18 cm while differences of both parameters of diamond-diode were within 0.06 cm. For the dose difference, the maximum of  $\delta_2$  and  $\delta_3$  of diamond-CC13 were 1.24 mm and 0.8%, respectively. The  $\delta_2$  and  $\delta_3$  of diamond-diode were 0.72 mm and 0.5%, respectively.

For small field sizes, the differences of  $RW_{50}$  and beam fringe between diamond and the others were within 2 mm. However,  $RW_{50}$  obtained by diamond detector were larger than the others in all field sizes studied. Beam fringe obtained by diamond detector were larger than those obtained by diode but smaller than those obtained by CC13. The penumbra obtained by diamond detector was 0.04 cm larger than those obtained by silicon diode. When compared to those by CC13, the penumbras obtained by diamond detector were smaller in all field size. The differences were 0.19, 0.17, 0.18, and 0.12 cm for field size of 4×4, 3×3, 2×2, and 1.5×1.5 cm<sup>2</sup>, respectively. For deviation between diamond-CC13, the maximum of  $\delta_2$  and  $\delta_3$  were 1.59 mm and 6.3%. For diamond-diode, the maximum of  $\delta_2$  and  $\delta_3$  were 0.6 mm and 1.7%. So, in all small field sizes studied,  $\delta_2$  and  $\delta_3$  of diamond-CC13 were always higher than diamond-diode.

**Table 4.10** Comparison of components of beam profiles of 6 MV photon beams obtained by diamond detector, CC13 ionization chamber, and silicon diode detector.

Field size (cm <sup>2</sup> )	$RW_{50}$ (cm)			Beam fringe 50-90% (cm)			Penumbra width 20-80% (cm)		
	Diamond	CC13	Diode	Diamond	CC13	Diode	Diamond	CC13	Diode
10x10	10.19	10.17	10.15	0.28	0.40	0.23	0.37	0.55	0.31
4x4	4.11	4.00	4.10	0.26	0.38	0.18	0.32	0.51	0.28
3x3	3.16	2.98	3.09	0.26	0.36	0.22	0.32	0.49	0.28
2x2	2.04	1.96	1.99	0.24	0.35	0.20	0.31	0.49	0.27
1.5x1.5	1.55	1.54	1.49	0.24	0.34	0.22	0.31	0.43	0.27

Table 4.11 The differences of beam profiles of 6 MV photon beams obtained by diamond detector, CC13 ionization chamber, and silicon diode detector.

Field size (cm <sup>2</sup> )	$\delta_2$ (mm)		$\delta_3$ (%)	
	CC13	Diode	CC13	Diode
10x10	1.24	0.72	0.8	0.5
4x4	1.59	0.33	2.2	1.0
3x3	1.13	0.58	1.5	1.7
2x2	1.51	0.51	6.3	0.9
1.5x1.5	1.23	0.60	5.0	0.6

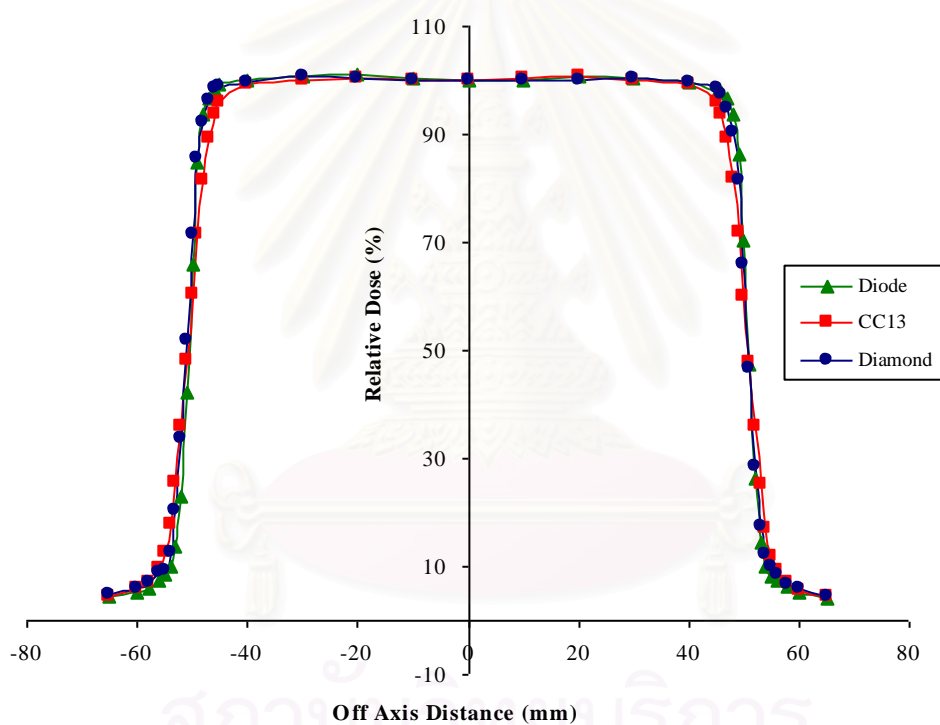


Figure 4.11 Beam profiles of 10×10 cm<sup>2</sup> of 6 MV photon beams obtained by diamond detector, CC13 ionization chamber, and silicon diode detector.

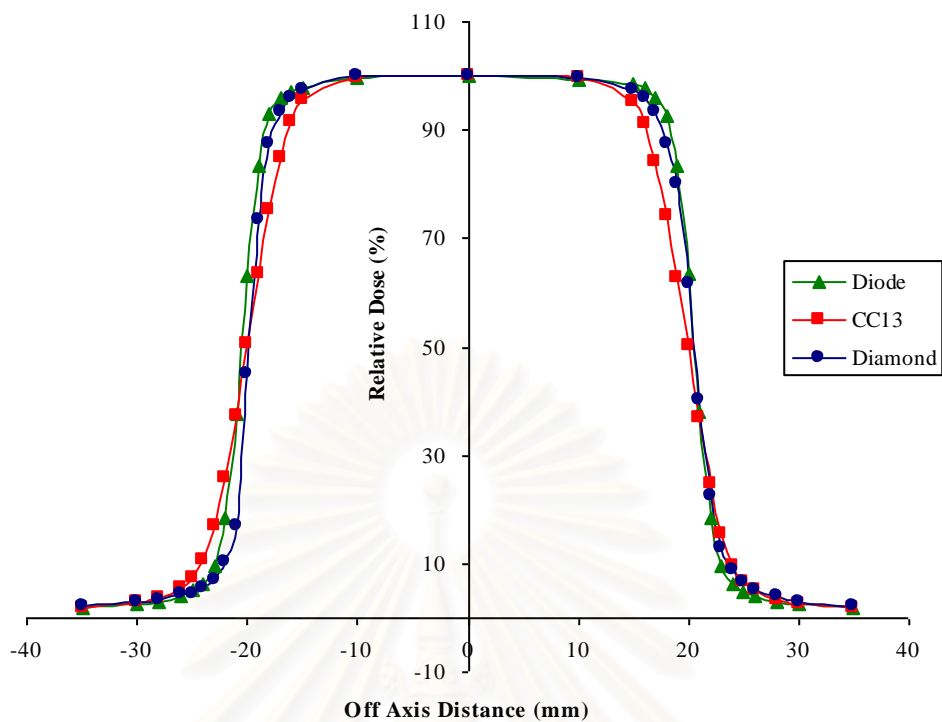


Figure 4.12 Beam profiles of  $4 \times 4 \text{ cm}^2$  of 6 MV photon beams obtained by diamond detector, CC13 ionization chamber, and silicon diode detector.

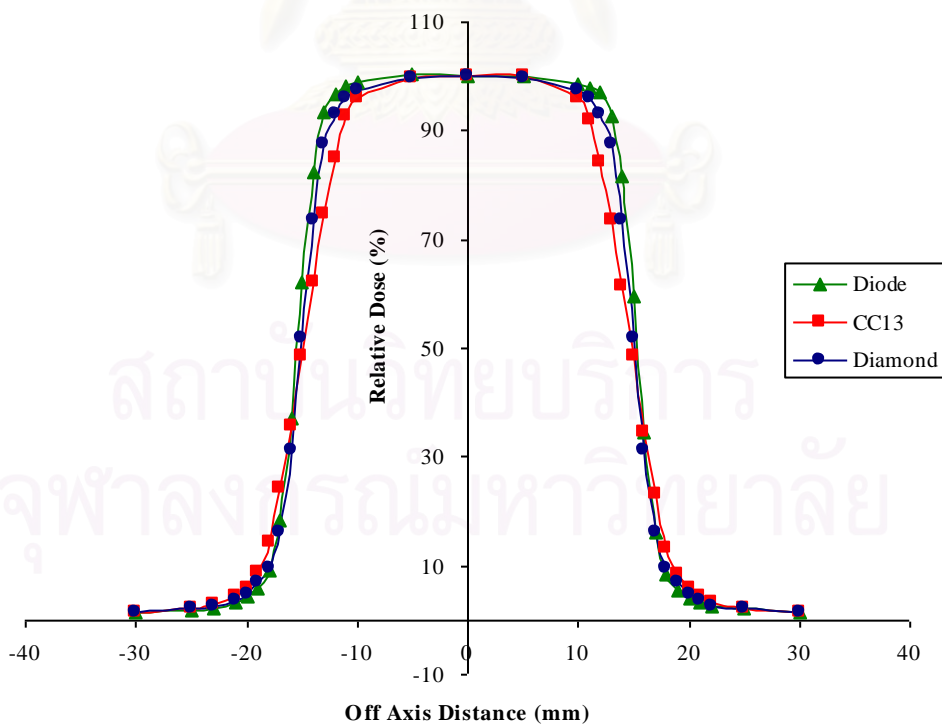


Figure 4.13 Beam profiles of  $3 \times 3 \text{ cm}^2$  of 6 MV photon beams obtained by diamond detector, CC13 ionization chamber, and silicon diode detector.

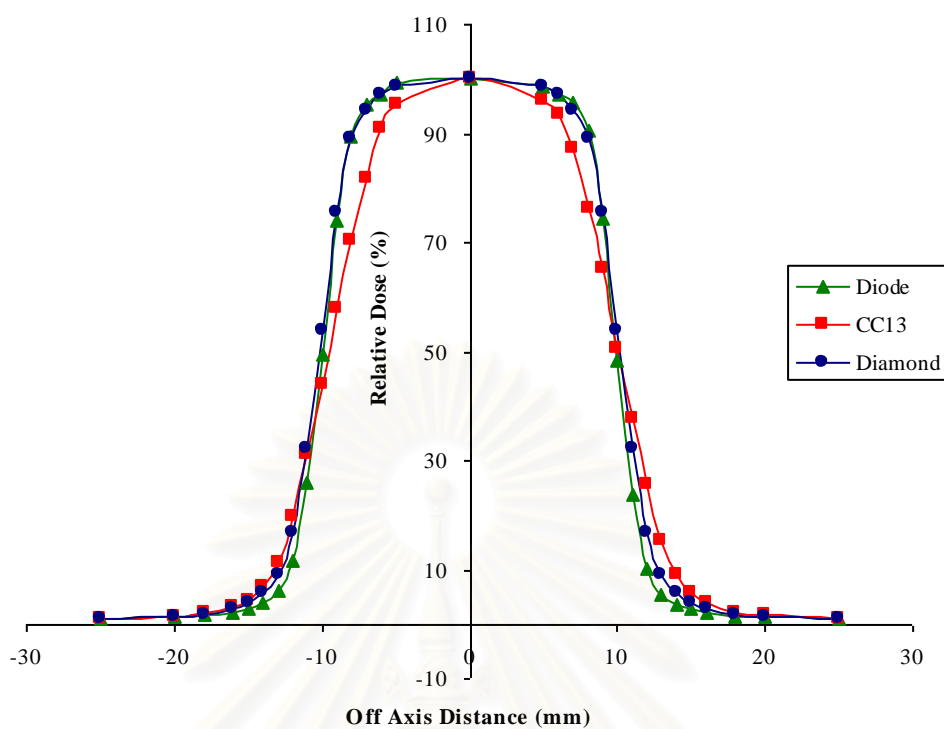


Figure 4.14 Beam profiles of  $2 \times 2 \text{ cm}^2$  of 6 MV photon beams obtained by diamond detector, CC13 ionization chamber, and silicon diode detector.

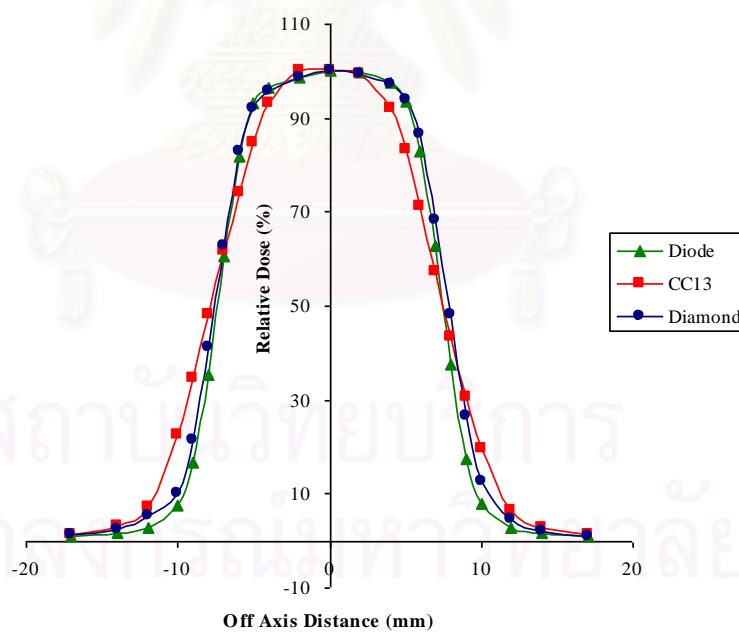


Figure 4.15 Beam profiles of  $1.5 \times 1.5 \text{ cm}^2$  of 6 MV photon beams obtained by diamond detector, CC13 ionization chamber, and silicon diode detector.



# CHAPTER V

## DISCUSSION AND CONCLUSION

### 5.1 Discussion

#### 5.1.1 Characteristics of Diamond Detector

In this study, the diamond detector shows idealistic characteristics such as high sensitivity, good repeatability, good reproducibility, and constant of response to the given dose. Although, slightly dependence on dose rate and beam directions were observed but diamond detector is independence to beam energy when compared to an ionization chamber which independence to beam energy.

With 5 Gy of pre-irradiation dose, many literatures [1,2,10,11,13,20] reported the same dose that is also suggested by manufacturer. However, pre-irradiation dose in PTW Measuring Probe Certificate might not be precise. De Angelis *et al*, [2] had reported a pre-irradiation dose of a diamond detector which was higher than suggested in PTW Measuring Probe Certificate, after they had found the differences of characteristics between two diamond detectors. Thus, the user should determine and attend to the pre-irradiation dose because it relates to the stability of detector response.

Although the diamond detector in this study had good repeatability but in practice, the response of detector was not stable when it was not irradiated for long period (more than 15 min) whether the bias was switched off or not. However, the variation of response was within 0.5% and there was returned to stable again after a few doses irradiation.

For dose rate dependence, the maximum variations of response were within 0.8 %, this number was valid only in dose rate range of 1.53-4.69 Gy/min, variations might increase if dose rate range increase. The dependence on dose rate due to very short electron-hole recombination time which related to the concentration of traps which gives more independence of detector conductivity with dose rate and lower the detector sensitivity to ionizing radiation. The relation of detector current with increasing dose rate can be described by

$$I = I_{\text{dark}} + R \times D^{\Delta}$$

where I is the diamond current, R is a constant of proportionality, D is dose rate,  $\Delta$  is the sublinear response parameter, and  $I_{\text{dark}}$  is the dark current of the detector. In this study,  $\Delta$  value was not used for correction because the response was slightly dose rate dependence. [20-21]

For the dependence on beam direction, the detector shows slightly directional dependence, unlike to the PTW manual which reported the independence on beam direction. Both De Angelis *et al* and Rustgi [2,13] showed agreement with our study, they also observed slightly dependence of detector on beam direction in parallel to

detector axis configuration. With limitation of gantry rotation to the couch, more deviation was expected when the angle is larger than  $120^\circ$  because the radiation beam will be interfered with the detector stem. In practice, the dependence on beam direction appears to be negligible factor in relative dosimetry measurement at the same condition unless using in off axis measurement.

### 5.1.2 Performance of Diamond Detector

For output factor measurement, differences of the output factors from different detectors were within 1% which was in the uncertainty of dose measurement, except in field size of  $1.5 \times 1.5 \text{ cm}^2$ , output factors obtained by CC13 was 2.3% lower than that obtained by diamond detector. Lower output factor of CC13 was due to lack of lateral electronic equilibrium in small field and averaging effect which obviously shows in beam profile measurement. With high spatial resolution and high sensitivity, the performance in output and beam profile measurement of diamond detector was superior to CC13 but comparable to silicon diode.

For depth dose curve measurement, depth dose curve obtained by diamond detector compared to those obtained by the others was higher in build up region but lower in descending region except for field size of  $1.5 \times 1.5 \text{ cm}^2$  which was lower in both regions. As expected, the depth dose curves obtained by silicon diode were overestimated in distal depth due to high sensitivity to low energy photons of silicon.

For beam profile measurement, diamond and diode were superior to CC13 with more sharp dose fall off at the edge of beam which demonstrated by smaller penumbra and beam fringe. There was not a significant problem in determination of field width because the reading of CC13 was averaged in small gradient or constant dose region of beam profile. So, both diamond detector and silicon diode were suitable and permitted a more accuracy determination of all parameters i.e. beam width, penumbras and beam fringes.

For IMRT technique, its beam consists of a number of small beam segments which was not only more complex but also has higher dose gradient than conventional beam. In high dose gradient, the response of a detector may differ substantially from absorbed dose. So, the volume averaging effect becomes more pronounced and leads to inaccuracy measurement particularly for large volume dosimeter. Moreover, electronic equilibrium within high dose gradient may not exist. [22] Thus the dosimetric measurements are to be made with achieve electronic equilibrium if the detector sensitive volume has significantly smaller than the beam. The measurement of beam data for used in IMRT planning with large volume dosimeter may leads to inaccuracy in both beam data and treatment planning. So, diamond detector and diode were suitable for this purpose. However, with nearly tissue equivalent property of diamond, the diamond detector was superior to silicon diode for dosimetric measurement for IMRT.

## 5.2 Conclusion

Diamond detector has suitable characteristics for used in small photon beam dosimetry. Pre-irradiation dose is need for stabilized detector response, so user should investigate for exact amount for each diamond detector. After pre-irradiation, detector has good repeatability and constant response, however, pre-irradiation is required if the detector dose not irradiate for a long period whether the bias was switched off or not.

Diamond detector and silicon diode, with high spatial resolution, are suitable choices of output and beam profile measurement in small photon beam whereas beam profiles determined by CC13 are more inaccurate with field sizes decrease due to the lack of lateral electronic equilibrium. For depth dose curve measurement, diamond detector and diode are suitable choices for small photon beams, CC13 is a good detector for larger field than  $3 \times 3 \text{ cm}^2$ . Measurement by diode will be resulted with overestimated in distal depth of depth dose curve especially for large field size.

For dosimetric measurement in IMRT, diamond detector and diode are suitable choices because they have small sensitive volume. However, with nearly tissue equivalent property of diamond, the diamond detector was superior to silicon diode.

## 5.3 Recommendation

For further study, application of diamond detector for specific patient quality assurance of complex treatments such as IMRT and Volumetric Arc Therapy (VMAT) should be observed for point dose verification.

## REFERENCES

- [1] Rustgi S. N., "Evaluation of the dosimetric characteristics of a diamond detector for photon beam measurement," Med. Phys. 22 (May 1995) :567 – 570.
- [2] De Angelis C., Onori S., Pacilio M., *et al.* "An investigation of the operating characteristics of two PTW diamond detectors in photon and electron beams," Med. Phys. 29 (February 2002):248-254.
- [3] Bucciolini M., Banci B. F., Mazzocchi S., De Angelis C., Onori S., and Cirrone G. A. P., "Diamond detector versus silicon diode and ion chamber in photon beams of different energy and field size," Med. Phys. 30 (August 2003):2149-2154.
- [4] Cember H., Introduction to Health Physics-2nd edition, (McGraw-Hill Inc.,1992).
- [5] Khan F. M., The Physics of Radiation Therapy-2nd edition, (Baltimore, ML: Williams&Wilkins, 1994).
- [6] Rosenfeld A. B., "Electronic dosimetry in radiation therapy," Radiation Measurement. 21 (2007) :s134-s153.
- [7] Barthe J., "Electronic dosimeter based on solid state detectors," Nucl. Instr. And Meth. In Phys. Res. B184 (2001):158-89.
- [8] [http://en.wikipedia.org/wiki/Material\\_properties\\_of\\_diamond](http://en.wikipedia.org/wiki/Material_properties_of_diamond)
- [9] Prasad R. R., "Diamond Radiation Detectors," (Alameda Applied Sciences Corporation, 2002).
- [10] McKerracher C., and Thwaites T. I., Notes on the construction of solid-state detectors,. Radiotherapy and Oncology 79 (2006) 348–351.
- [11] Ciancaglioni I., Consorti R., Rossi M. C., and Conte G. "Polycrystalline diamond detectors compared with silicon X-ray dosimeters for clinical," IEEE 7 (2004):4445-4447.
- [12] Bergonzo P. *et al.* "Improving diamond detectors: A device case," Diamond & Related Materials 16 (2007):1038–1043.
- [13] Rustgi S. N., Frye D. M. D., "Dosimetric characterization of radiosurgical beam with diamond detector," Med. Phys. 22 (December 1995):2117-2121.
- [14] PTW Diamond Detector Type 60003 User Manual, (Freiburg).
- [15] "AAPM Report NO.46 Comprehensive QA for Radiation Oncology". Med. Phys. 21 (April 1994):581-618

- [16] IAEA, TRS-398 Absorbed Dose Determination in External Beam Radiotherapy: An International Code of Practice for Dosimetry based on Standards of Absorbed Dose to Water, (IAEA 2004).
- [17] Van Dyk J., Barnett R. B., Cygler J. E., and Shragge P. C. "Commissioning and quality assurance of treatment planning computers," Int. J. Radiat. Oncol. Biol. Phys. 26 (1993):261-273.
- [18] "AAPM Radiation Therapy Committee Task Group 53:Quality assurance for clinical radiotherapy treatment planning," Med. Phys. 25 (October 1998):1773-1829.
- [19] Venselaar J. *et al.*, "Tolerances for the accuracy of photon beam dose calculations of treatment planning systems," Radiotherapy and Oncology 60 (2001):191-201.
- [20] Laub W. U. *et al.* "Energy and dose rate dependence of a diamond detector in the dosimetry of 4–25 MV photon beams," Med. Phys. 24 (April 1997): 535-536.
- [21] Fidanzio A. *et al.*, "PTW-diamond detector: Dose rate and particle type dependence," Med. Phys. 27 (November 2000):2589-2593.
- [22] NiZin P.S., "Electronic equilibrium and primary dose in collimated photon beam," Med. Phys. 20 (June 1993):1721-1729.



## VITAE

**Name** Mr. Paya Thantaranont

**Date of Birth** October 10, 1978

**Place of Birth** Bangkok, Thailand

**Institution Attended** Faculty of Science, Ramkumhang University,  
Bachelor of Science (Radiological Technology), 2004  
Faculty of Medicine, Chulalongkorn University,  
Master of Science (Medical Imaging), 2008

**Position held & Office** 2000 to present  
Department of Radiotherapy  
Chonburi Cancer Center ,  
Chonburi, Thailand

**Position** Radiological Technologist

**Present address** 9/6 Rimtangrod fai, Bangkok, Jomtong, Bangkok 10150



สถาบันวิทยบริการ  
จุฬาลงกรณ์มหาวิทยาลัย



สถาบันวิทยบริการ  
จุฬาลงกรณ์มหาวิทยาลัย